

## Review Article

Yueqian Zhang\* and Herbert Gross

# Systematic design of microscope objectives. Part II: Lens modules and design principles

<https://doi.org/10.1515/aot-2019-0013>

Received January 22, 2019; accepted April 23, 2019; previously published online June 7, 2019

**Abstract:** Based on the microscope objective database and systematic classification introduced in Part I, the Zones 1–4 objective lenses are systematically analysed in this paper to extract the building blocks. All the definitions and terms are based on the preceding paper. The lens modules utilised in the front, middle and rear groups are investigated by reliable aberration evaluation tools with robust and accurate raytracing. Thereby, the aberration correction principles are summarised, from which 29 lens modules are well sorted with respect to their decoupled aberration correction functionalities. Furthermore, some intrinsic relations between the aberration-related lens modules and the impact of applications or the consideration of manufacturing and technology are also discussed. Utilising the lens modules, system modification and synthesis examples shall be given in Part III.

**Keywords:** aberration correction; microscope objective; microscopy; optical design.

## 1 Introduction

According to the methodology of the systematic analysis of microscope objectives, which was introduced in Part I [1], the phenomenological Epoché should be operated to decouple the impacts of aberration correction, application, manufacture and technology. As the first step, we have proposed a systematic classification for most of the patented systems based on the historical review of lens evolution and summarised the major manufacture

considerations and the impact of applications in Part I. However, it only provides the framework of the systematic analysis and discusses the impacts marked by red arrows in Figure 1, which illustrates the relationships between the three factors. The impacts of the applications on system parameters have been well summarised, but some direct impacts on lens modules have not been introduced in detail, along with the direct impact of the manufacturing and technology considerations on each lens module. Furthermore, the relationship between the system parameters and the corresponding aberration correction strategies has yet to be introduced as well. Hence, the functionality of lens modules in the aberration correction remains unclear.

In the previous literature, a systematic analysis of the lens modules is missing [2]. The design principles of special lens structures are only briefly introduced in some patents. Therefore, the second step presented in the current paper is to extract the lens modules and illustrate the design principles of the microscope objectives, particularly regarding their direct relation with the aberration correction, applications, manufacture and technology. Concerning the aberration correction, as the most important aspect, the general aberration behavior resulting from the system parameters of microscope objectives is first summarised, and the correction strategy of each aberration is discussed in Section 2. With appropriate tools for aberration calculation, the general power distribution and material selection principles are introduced in Section 3. To demonstrate the lens modules more clearly, in this paper, we focus on the microscope objectives from Zones 1–4, which generally consist of two or three groups with distinctive functionalities. The detailed lens modules utilised in the front, middle and rear group are discussed in Sections 4–6, respectively. In our database with 484 microscope objectives, there are 443 entries (91.5%) classified into Zones 1–4. According to the classification in Section 4 of Part I, the systems are further classified based on their colour correction, field correction, working distance and correction function (CORR). Concerning each class, the summarised lens modules and design principles are valid in more than 80% of the examples. The special design principles

\*Corresponding author: Yueqian Zhang, Institute of Applied Physics, Friedrich Schiller University Jena, Albert-Einstein-Str. 15, 07745 Jena, Germany, e-mail: yueqian.zhang@uni-jena.de

Herbert Gross: Institute of Applied Physics, Friedrich Schiller University Jena, Albert-Einstein-Str. 15, 07745 Jena, Germany

[www.degruyter.com/aot](http://www.degruyter.com/aot)

© 2019 THOSS Media and De Gruyter

 Open Access. © 2019 Yueqian Zhang et al., published by De Gruyter.  This work is licensed under the Creative Commons Attribution-NonCommercial-NoDerivatives 4.0 License.

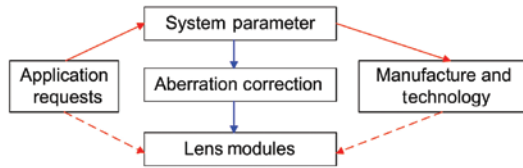


**Figure 1:** Relationships between the three major factors that influence the lens modules: Aberration correction, application requests and manufacture and technology.

utilised in the Zone 5 very-low-magnification systems and Zone 6 very-high-magnification systems will be discussed in Part III.

## 2 Analysis tools and overview of aberrations

The microscope objective is the most characteristic aperture-dominant optical system with high numerical aperture (NA) and small field size. Due to the high NA, the raytracing method should be carefully defined to assure reasonable pupil setting for both real and paraxial rays. Based on the accurate real and paraxial raytracing, the aberrations should be calculated accurately, especially regarding the higher-order behaviour. Particularly in the modern microscope systems with epi-illumination, the light beam passes through the objective lens from both directions. To check both side performance and to avoid the possible impact of the higher-order induced aberrations, the raytracing and aberration evaluating method should be robust to handle both the tracing from high NA to low NA and from low NA to high NA. Furthermore, in order to extract the lens modules, the analysis tool should also be capable of evaluating the contributions of both surfaces and lens groups to the aberration correction.

In this section, the raytracing method and aberration analysis tools are first clarified. Utilising the tools, the general aberration behaviour of the microscope objectives is then summarised. Hence, to extract lens modules, the intuitive structural groups and the functional aberration-correcting groups could be related, which is helpful in dividing the microscope objectives into the front, middle and rear groups for further analysis.

### 2.1 Raytracing method and higher-order aberration analysis

In an optical system fulfilling the sine condition, the pupil has a spherical shape. This is typically simplified

to a pupil plane for raytracing. However, when the object space NA is larger than 0.5, the raytracing error resulting from the pupil shape cannot be neglected. High NA microscope objectives are typically well corrected for the offence against sine condition (OSC). Therefore, to achieve accurate real ray data for aberration calculation, the raytracing method should be able to find the real shape and size of the pupil. Popular commercial optical design software utilised different methods to determine the real pupil. In Zemax/OpticStudio™, for high NA systems, the ‘real ray aiming,’ which utilises iterative raytracing to match the edge of the aperture stop and the real pupil, should be activated. A more general method to accurately scale and normalise the object and image space aperture is to define the canonical pupil coordinates as proposed by Hopkins [3]. In OSLO, as the default setting, the ‘aplanatic ray aiming’ is utilised to specify the real rays, which is based on the canonical coordinates. Code V also implemented the canonical coordinates, thus defining the energy-conserved object and image space for the optical systems fulfilling the sine condition.

When either of these two methods is applied in the analysis of microscope objectives, real ray data can be accurately obtained. Apart from the slight influence of induced aberration, the real ray data are nearly consistent when the rays are traced from different directions, namely, from high NA object space to low NA image space or from low NA image space to high NA object space. However, concerning the paraxial raytracing, the paraxial marginal ray angle is determined by the pupil edge on the pupil plane instead of the pupil sphere. Consequently, paraxial raytracing, which is also important in aberration calculation, cannot be operated under the spherical pupil settings mentioned above. Regarding the microscope objectives, when the rays are traced from the low NA image space to the high NA object space, due to the small deviation at the edge of the planar and spherical entrance pupil, the paraxial raytracing is rather accurate. However, when the raytracing direction is reversed, the paraxial object space NA becomes too large, resulting in unrealistic or inconsistent paraxial ray data. This is also one of the reasons why the microscope objective lenses are conventionally designed inversely. The low NA image space is considered as the object space and the high NA object space is treated as the image space.

Therefore, to analyse the aberration behaviour of the microscope objective lenses, including the higher-order induced aberration, the consistent paraxial raytracing method should be implemented and incorporated with accurate real raytracing to evaluate the aberrations. We propose a special iterative paraxial raytracing method

in Zemax/OpticStudio™ to achieve realistic and nearly consistent paraxial ray data, independent of raytracing direction. Compared with the conventional methods, marginal ray tracing using the new approach is schematically illustrated in Figure 2. The RONA and RINA indicate the real object space and image space numerical apertures, respectively, whereas the PONA and PINA refer to the corresponding paraxial object space and image space numerical apertures. The  $h_r$  and  $h_p$  demonstrate the real marginal ray height and paraxial marginal ray height, respectively, and the EnP and ExP present the corresponding positions of the entrance pupil and the exit pupil. In addition, the blue sphere demonstrates the real pupil fulfilling the sine condition, whereas the red plane gives the paraxial pupil plane under paraxial approximation.

In Zemax/OpticStudio™, there are six aperture types to define the aperture size of the optical system. Given

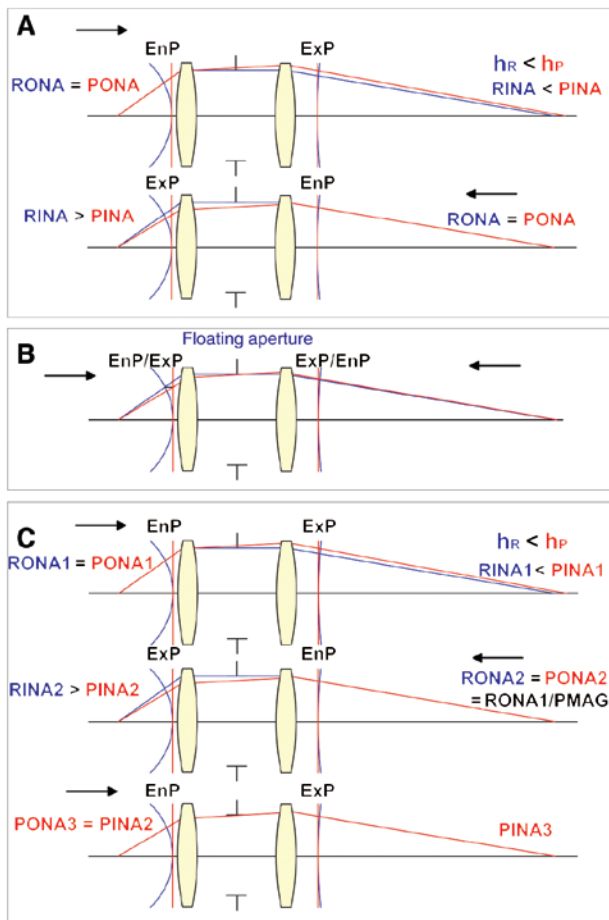


**Figure 2:** Comparison of the three raytracing methods. (A) Conventional raytracing method. The aperture is set by object space NA. (B) Conventional raytracing method. The aperture is defined by the floating aperture stop size. (C) The iterative raytracing method with three iterations. The aperture is set by object space NA.

that the apertures of the microscope objectives are always specified by NA, it is intuitive to use the object space NA (ONA) to define the aperture for the conventional raytracing method (A). Under this circumstance, the software set the real object NA (RONA) and paraxial object NA (PONA) identical as the given value. Therefore, for the high NA systems, the paraxial angle can exceed the theoretical maximum value of 0.707. Consequently, the following paraxial ray heights might be far larger than the real ray heights, which is an unrealistic scenario. When the raytracing direction is reversed, the new RONA and PONA could be set with the low NA, which can be calculated as the objective specified NA divided by the paraxial magnification. The paraxial magnification could then be obtained from the paraxial chief ray tracing from the high NA side to the low NA side, which is reliable due to the small field size. As the deviations of the real and paraxial entrance pupils on the low NA space are very small, the resulting paraxial image space NA (PINA) on the high NA side could represent the practical paraxial aperture, which is smaller than the real image space NA (RINA). Utilising the conventional method (A), the real raytracing is quasi-consistent, whereas the paraxial raytracing is prone to large errors.

To keep the real raytracing and paraxial raytracing consistent for different raytracing directions, the conventional method (B) utilises the type 'Float by STOP size' to define aperture size. When the 'real ray aiming' is activated, the boundary of the aperture STOP, the spherical entrance pupil and the spherical exit pupil are conjugated with the real raytracing. Both the real and paraxial marginal ray tracing start from the aperture STOP, which is located in the middle of the systems; therefore, the paraxial ray height  $h_p$  and real ray height  $h_r$  on the aperture STOP are identical. However, it is self-evident that the fulfilment of the 'real ray aiming' and 'paraxial ray aiming' cannot be achieved simultaneously. As the real ray aiming is activated to assure the accurate real raytracing, the paraxial pupil edge cannot be accurately found. Therefore, although the resulting paraxial ray data are quasi-consistent for different raytracing directions, they might reach unrealistic values when the system has extremely high NA, e.g.  $NA > 0.9$ .

In the new approach (C), the first two steps of raytracing are identical to the conventional method (A), but after the PINA2 is achieved according to the raytracing from the low NA side to the high NA side, it is used as the ONA again to trace the paraxial ray back with the activation of the paraxial ray aiming. The obtained paraxial ray data are quasi-consistent compared with the second step raytracing. To further improve the accuracy of the paraxial NA, the obtained PINA3 could be further

used as the RONA4 = PONA4 and then the raytracing is operated from the low NA side to the high NA side again for the next iteration. However, typically only with demonstrated three steps, the accuracy of the paraxial data is sufficient to accurately evaluate the aberrations.

As a conclusion, when the microscope objectives are analysed in Zemax/OpticStudio™, to calculate the aberrations, the real ray aiming is activated for accurate real raytracing, and the iterative paraxial raytracing is operated to achieve the paraxial ray data. Notably, a similar approach could also be applied in OSLO and Code V, where the canonical coordinates are implemented to trace the real ray. By operating an additional paraxial raytracing with the ideal pupil setting and combing the paraxial ray data with the real ray data to calculate the aberration, the realistic and quasi-consistent aberration behaviour of the microscope objectives could be determined.

In order to understand the functionality of the lens modules for aberration correction, the Seidel coefficients, which can be decomposed to the surface contribution, are utilised to evaluate the primary aberrations. Due to the physical nature and correction strategy of the aperture-dominant system, which shall be discussed in Section 2.2, the Seidel aberration is sufficient to evaluate the field aberrations (only except some extremely high NA cases). To evaluate the correction of the axial field, the Delano formula, shown in Equation (1), is utilised to calculate the exact full-order spherical aberration (SA) and its surface contribution [4]

$$\Delta s'_{\text{SPH}} = \Delta s_{\text{SPH}} \cdot \frac{n_1 u_1 \sin U_1}{n'_k u'_k \sin U'_k} + \sum_j \frac{n_j}{n'_k} \cdot H_j \cdot \sin \frac{I'_j - I_j}{2} \cdot \frac{2i_j \cdot \sin \frac{I'_j - U_j}{2}}{u' \sin U'_k}. \quad (1)$$

Thus, the critical higher-order SA (coefficient) contribution  $S_{\text{HSPH}}$  resulting from the high NA could be determined by subtracting off the Seidel contribution  $S_I$  from the full-order contribution  $S_{\text{FSPH}}$ , as shown in Equation (2)

$$S_{\text{HSPH}} = S_{\text{FSPH}} - S_I = \sum_j 4n_j H_j i_j \sin \frac{I'_j - I_j}{2} \sin \frac{I'_j - U_j}{2} - \sum_j n_j h_j i'_j (i'_j - i_j) (i'_j - u_j), \quad (2)$$

where the  $H$  in the full-order contribution represents the chord length between the incidence point and the vertex of the surface, and the  $h$  in the Seidel contribution is the height of the incidence point with the reference to the

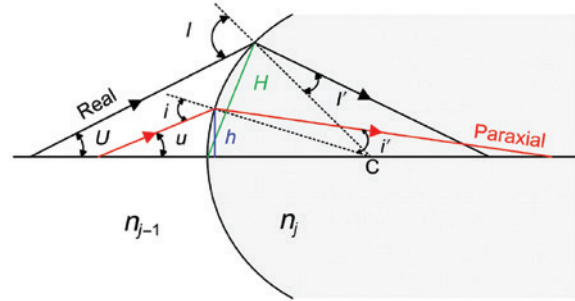


**Figure 3:** Raytracing data for SA contribution calculation. The capital letters refer to the real ray data, while the small letters refer to the paraxial ray data.

optical axis. All the raytracing data used in Equations (1) and (2) are schematically demonstrated in Figure 3.

The primary, higher-order and full-order SA coefficients of an example 100×/0.95 microscope objective [5] are calculated, as shown in Figure 4. A 200 mm tube lens is placed behind the infinite-conjugate objective to form the intermediate image with low image space NA = 0.0095. The higher-order induced aberration due to the raytracing direction can be analysed by comparing the corresponding surface contributions.

The SA according to the different raytracing directions are nearly consistent. The slight differences of the higher-order SAs can only be seen on surfaces 1, 7, 8, 10 and 13, which are the special structures with extraordinary higher-order aberration behaviours, such as strongly curved cementing surface or air lens. The details of these lens modules will be introduced in Sections 4 and 5. The induced aberration due to the raytracing direction is not critical in most of the microscope objectives. The ability to maintain identical performance for different raytracing directions is an advantageous feature of the microscope utilising epi-illumination.

When it comes to the chromatic aberrations, the basic contributions can also be analysed with the Seidel approach. For the Apochromate lens and the systems corrected for the extended spectrum (class (c) to class (g) defined in Part I), the secondary and even higher-order spectrum is evaluated by calculating the additional colour. In high NA objectives, the spherochromatism significantly affects the system performance when the effective NA is narrowed. Therefore, it is also corrected in the recently developed objectives with high performance. To analyse the functionality of the lens modules in correcting spherochromatism, the third-order spherochromatism surface contribution [6] is utilised.

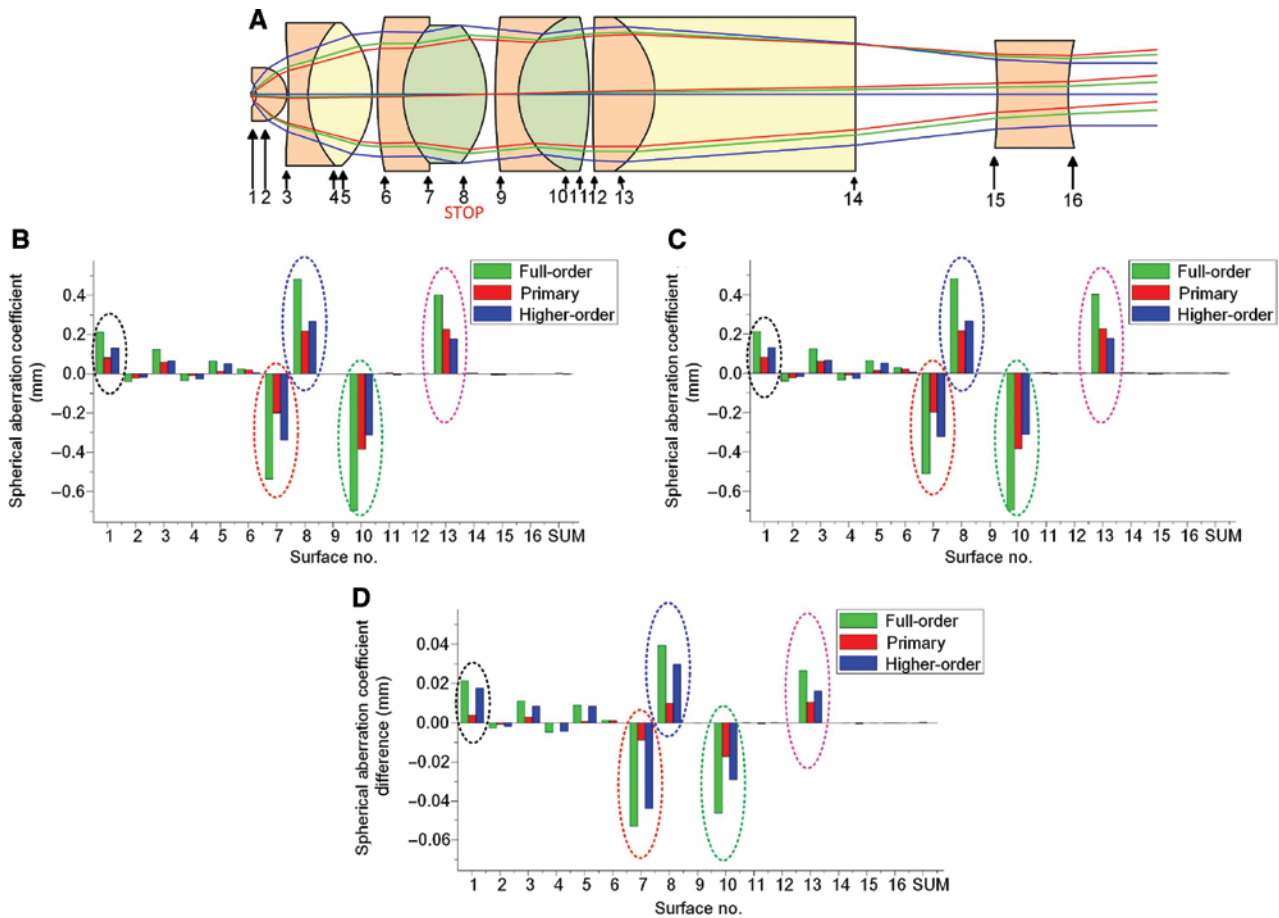


**Figure 4:** The SA of the example 100 $\times$ /0.95 objective. (A) System layout with surface number. (B) Surface contributions calculated by raytracing from the object side to the image side. (C) Surface contributions calculated by raytracing from the image side to the object side. (D) Difference between the SA contributions calculated under the case (B) and case (C).

## 2.2 Overview of the aberrations and their correction strategies

The five monochromatic and two chromatic primary aberrations as well as the higher-order SA and spherochromatism can be compared in terms of their distinctive correction strategies. Notably, except for the very-low-magnification objectives in Zone 5, the distortion has little effect on the system performance due to the small object field size. Therefore, in this paper, the distortion correction is neglected, and its behaviour in Zone 5 systems will be introduced in Part III.

Before the invention of the Plan-objectives, the general aberration correction strategy for microscope objectives have been well described [7] and classified into two basic types. For one thing, the SA, coma and axial chromatic aberration (ACA) should be corrected at the source, where they are generated. Therefore, according to the introduction in Part I, the conventional two-group Lister or Amici type objectives utilised an aplanatic lens

with achromatic cementing to control these three aberrations. For the other, the astigmatism and lateral chromatic aberration (LCA) should be compensated by remote lens groups. Before the invention of infinity optics, they are usually corrected by the eyepiece or a remote rear group in the objective. A different compensation strategy of these two aberrations significantly influenced the design of infinity optics in the standardised microscopes from different vendors.

The first Plan-objective with field curvature (FC) correction was invented by Boegehold [8], who introduced a thick meniscus lens as a rear group. The general correction strategy of the FC belongs to the second type, based on the compensation between remote groups. However, according to the objective evolution, when the system etendue increases, particularly due the large NA, correcting the tremendous SA and ACA within a single element or single lens group is no longer feasible. Therefore, the residual error should also be compensated by different lens groups. Moreover, due to the increasing field, the

coma should be compensated as well. Another specific effect induced by the high NA and large field is the higher-order contribution, but its correction strategy for SA and coma are different. The higher-order SA is inevitable when the NA is larger than approximately 0.5. To correct the full-order SA, the higher-order contribution should be utilised to compensate the lower-order contribution instead of eliminating it. Therefore, the compensation of both the primary and higher-order SA is considered during the system design. When it comes to coma, on the contrary, its higher-order contribution should be typically restrained at the source, while the primary contribution is compensated by different groups [9]. This is realised by the appropriate selection of a rear group structure, where the chief ray height is large, thus generating higher-order coma.

According to these correction strategies, in order to analyse the functionality of the lens modules, the full-order SA and Seidel contribution of all the aberrations are analysed. Regarding the group functionality, Table 1 presents a comparison of five representative objectives belonging to the Zone 1 two-group objective, Zone 1/2 double-Gauss type objective, Zone 2 clear-three-group objective, Zone 3 novel three-group objective and Zone 4 extremely high etendue objective, respectively. According to the historical review in Part I, the rear group in the two-group system mostly plays the role of the middle group in the three-groups systems.

The correction strategy of the SA is the most complicated, which could be generally classified into three types:

1. The middle group compensates nearly all the SA introduced by the front group
2. The middle group and rear group correct the SA together
3. The rear group corrects most of the SA

Systems (a) and (d) belong to the Type 1 correction, where the front lens structure violates the aplanatic condition, but it has better control of the chromatic aberration. Therefore, a great amount of residual SA is introduced, which should be compensated by the middle group (or rear group in the two-group system) with large ray height.

Type 2 is most commonly used in the Zones 1–3 systems, such as systems (b) and (c). The front lenses nearly fulfil the aplanatic condition, thereby only introducing a small amount of SA but with large residual ACA. The middle group, which consists of several cemented doublets or triplets with appropriate glass selection, can perfectly correct the ACA but it is sometimes difficult to control SA simultaneously. Consequently, the residual SA must be corrected by the rear group with large ray height. Comparing systems (a) and (b) with (c) and (d), apart from

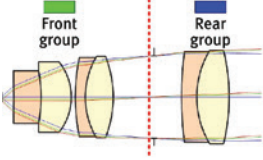
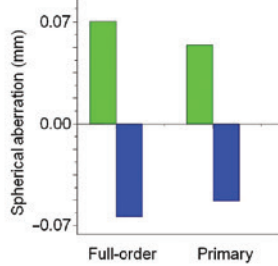
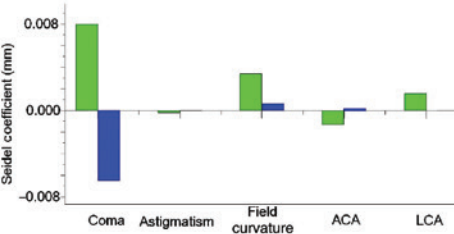
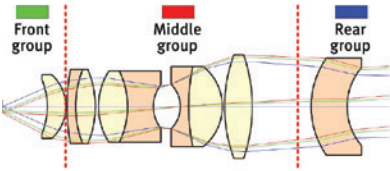
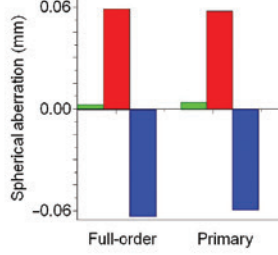
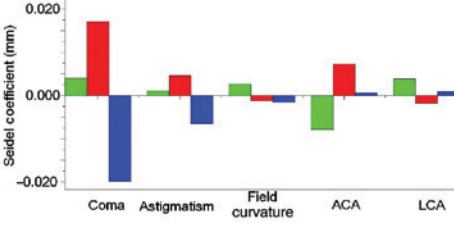
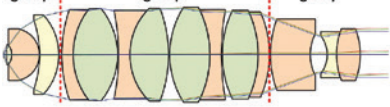
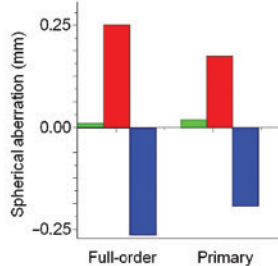
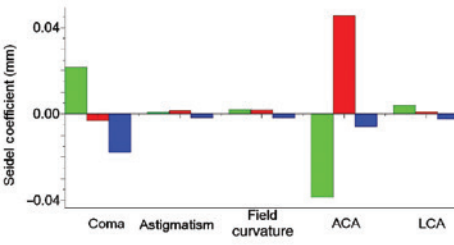
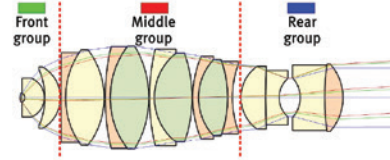
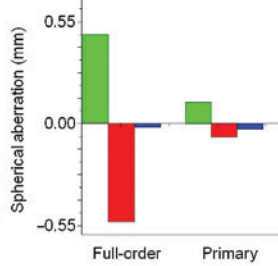
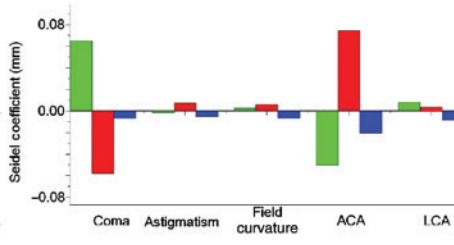
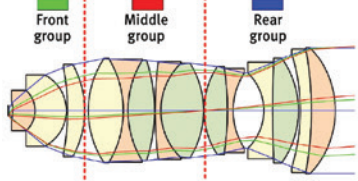
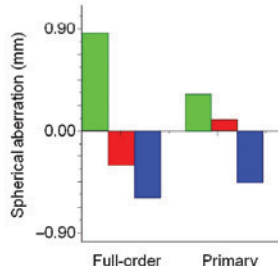
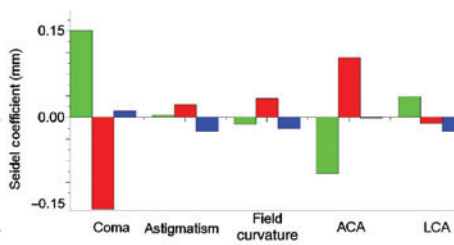
the different compensation strategies, we can also see the difference between ‘correction at source’ and ‘correction by compensation’. In systems (a) and (b), due to the relatively small NA, it is feasible to control the SA in both the front group and middle (rear) group small. Therefore, although the well-corrected SA is realised by compensation, the contributions of the two parts are relatively small. On the contrary, due to the high NA, systems (c) and (d) must leave a large contribution in the two groups for compensation. Consequently, they have far more critical alignment sensitivity than systems (a) and (b).

Type 3 is widely utilised in the recently developed microscope objective with extended NA and etendue, e.g. system (e). The tremendous SA from the front group is inevitable, particularly for dry objectives. The residual error should be compensated by both the middle group and the rear group. To control the coma associated with OSC simultaneously and to avoid generating its higher-order contribution, the rear group, where the heights of chief ray and coma rays are large, should be designed so that they are nearly free of coma. Hence, the middle group mostly compensates the coma, whereas the rear group mostly corrects the SA.

Concerning the higher-order behaviour, in the Zones 1 and 2 systems (a) and (b), due to the relatively small NA, the primary contribution dominates the SA. In the Zone 2 objectives with high NA, such as system (c), although there is larger higher-order SA introduced by the large aperture, it is compensated between the middle and rear groups, which is identical to the primary SA compensation. When it comes to the high NA system with increased etendue, the higher-order contribution should be utilised to correct the high aperture, particularly to restrain the zonal error [zonal spherical aberration (ZSA)]. Therefore, the full-order compensation is distinctive to the primary SA compensation, which can be observed from systems (d) and (e). This effect could be realised by specific features, such as an air lens or special cementing.

There are also various coma correction strategies, which can be basically classified as two types: correction in the rear group and correction in the middle group. When the system etendue is relatively small (Zones 1–2), given that the chief ray height at the rear group is large, it is feasible to compensate the coma with a lens group with strong optical power, particularly with thick meniscus lenses, which is also beneficial to FC correction. This compensation behaviour can be found in systems (a), (b) and (c). However, when the etendue increases, the exit pupil size is enlarged, resulting in the large coma ray height in the rear group. To avoid the tremendous coma introduced by the asymmetric coma rays, especially to vanish the higher-order contribution, one method

**Table 1:** Representative objectives from each etendue zone with comparable aberration correction strategy.

Objective system	Spherical aberration	Field and chromatic aberrations
<p>(a) Zone 1 two-group 40×/0.65 SF18 Uetake USP 3623792</p> 		
<p>(b) Zone 1/2 double-Gauss 20×/0.40 SF31 Matsubara USP 3925910</p> 		
<p>(c) Zone 2 clear-three-group 100×/1.30 O SF12 Shoemaker USP 3700311</p> 		
<p>(d) Zone 3 novel three-group 40×/1.20 W SF23 Okuyama USP 2003-0043473</p> 		
<p>(e) Zone 4 extremely high etendue 10×/0.90 SF25 Fujimoto USP 8350904</p> 		

The ACA and LCA are calculated for the F-line to C-line.

is to introduce vignetting to reduce the off-axial effective NA by cutting off the coma rays. Another method to completely correct coma is to design the rear group with relatively small optical power and quasi-symmetric structure. Due to the high

NA, although the chief ray height is low in the middle group, it can still generate a significant contribution for coma compensation. The systems (d) and (e) use both vignetting and quasi-symmetric rear group to restrain coma.

According to Table 1, the astigmatism in the microscope objective is usually not critical. It is slightly introduced in the front and middle groups and compensated by the rear group.

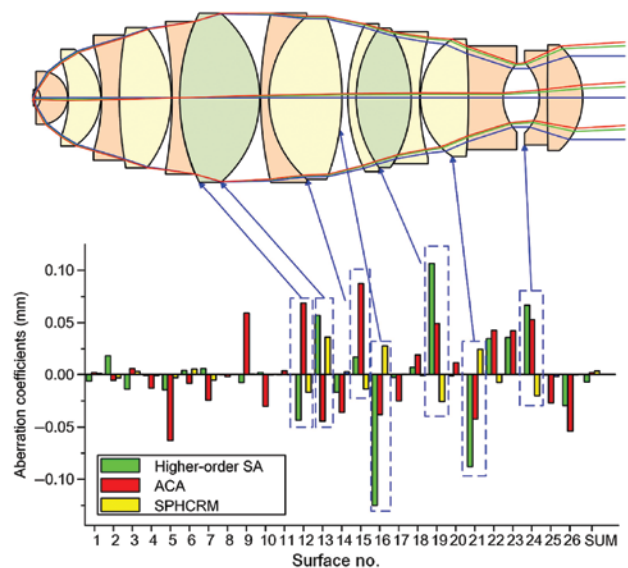
When it comes to the FC correction, in the conventional microscope objectives, to achieve the large magnification, the front and middle groups are designed with strong positive optical power, resulting in a negative Petzval curvature. To compensate the FC, one method based on Petzval's theorem is to use a remote negative lens group for compensation. Boegehold introduced another method, which utilises thick meniscus lens with appropriate curvatures to generate a positive Petzval curvature (negative Seidel contribution) with arbitrary optical power. In the modern microscope objectives, these two methods with complicated structures are widely used. The quasi-symmetric rear groups consisting of several meniscus lenses are typically designed with negative power, which is also beneficial in correcting coma and astigmatism. However, there are two special exceptions. First, the double-Gauss structure, which is widely used in low NA long working distance objectives, could correct the Petzval curvature with its symmetric meniscus lenses. According to system (b), both the double-Gauss middle group and single meniscus rear lens generate a positive Petzval curvature, which is used to compensate the large residual error from the front quasi-aplanatic lens. Second, it is notable that the embedded lens, which is widely used in the immersion objectives, could also introduce a positive Petzval curvature with positive optical power. In system (e), although it is a dry lens, an embedded front lens is also utilised, generating significant positive Petzval curvature. This special feature will be introduced in detail in Section 4.

In almost all the systems, the correction strategy of the ACA is the same. The front group always introduces a certain amount of ACA, which must be corrected by the middle group. In the conventional system, the rear group is nearly free of ACA. However, when the thick lenses are used in the rear group, particularly containing high dispersive dense flint (SF) glasses with large marginal ray height, the rear group can also contribute to the ACA correction.

In the standardised microscope systems, different vendors have different strategies to correct the lateral chromatic aberration (lateral colour). Systems (a) and (b) are designed for a traditional objective with finite tube length, where the lateral colour is compensated by the eyepiece. Therefore, according to Table 1, there is a large residual lateral colour. The systems (c), (d) and (e) were designed for the standardised microscope system with infinity optics from American Optical Corporation, Nikon and Olympus, respectively. All the three vendors fully correct the lateral

colour in both the objective and tube lens, which is typically realised by the great compensating contribution of the rear group. Some other vendors, such as Leica and Zeiss, leave a certain amount of lateral colour in the objective and compensate it in the tube lens. Under this circumstance, the rear group is utilised to control the lateral colour to the standardised value instead of eliminating it. Before the introduction of infinity optics, involving the lateral colour compensating functionality into the rear group could lead to great burden for optical design. However, in the modern systems, the functionality of the coma and FC correction dominates the complexity of rear group and the lateral colour correction becomes less influential.

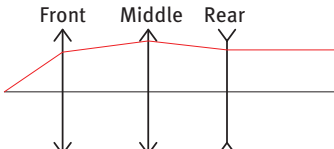
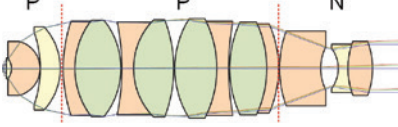
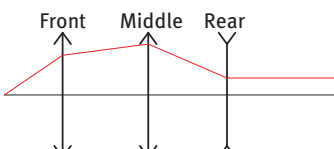
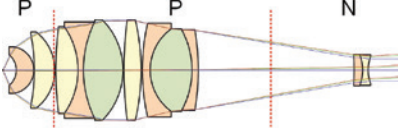
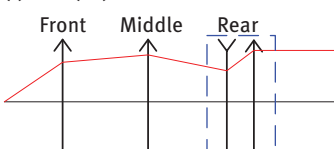
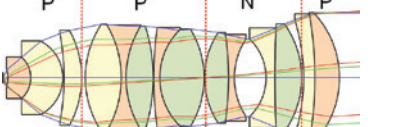
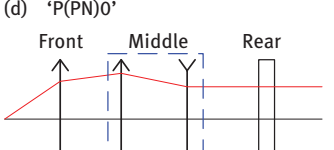
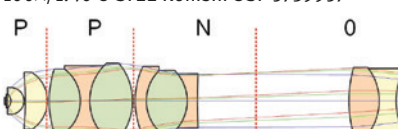
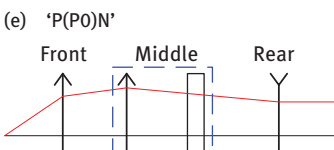
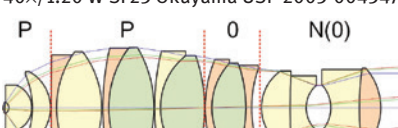
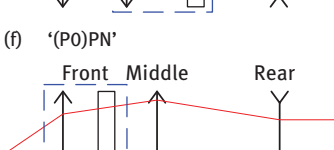
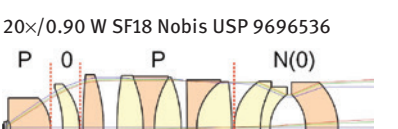
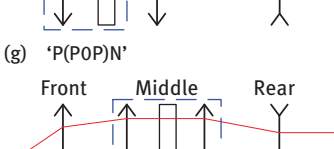

In recent high NA Apochromate objectives, particularly for fluorescence microscopy with laser excitation, the spherochromatism is also well corrected. The correction strategy of spherochromatism is complicated but could be understood by induced effect [6, 10]. Generally, the significant spherochromatism contribution always comes together with a large contribution of higher-order SA and ACA, which could be seen from the example 55.9×/1.40 oil immersion objective with perfect spherochromatism correction [11] shown in Figure 5, which is the same as the system (d) in Table 2 of Part I. The spherochromatism is mostly corrected in the middle and rear group by lens modules with extraordinary higher-order aberration, such as air lens and special cementing. In this paper, we mainly focus on the major correction behaviour in the middle group.



**Figure 5:** Surface contribution of higher-order SA, ACA (F-line to C-line) and spherochromatism (F-line to C-line) of the 55.9×/1.40 oil immersion objective [11] with perfect spherochromatism correction.



**Table 2:** Representative objectives belonging to the typical seven types of optical power distribution.

Power Distribution type	Example system	Retrofocus factor $r$
(a) 'PPN' 	100×/1.25 O SF12 Shoemaker USP 3700311 	0.25–0.8
(b) 'PPN strong retrofocus' 	100×/0.90 LD SF25 Hiraga JP 2000-241710 	<0.25
(c) 'PP(NP)' 	10×/0.90 SF25 Fujimoto USP 8350904 	>0.8
(d) 'P(PN)0' 	100×/1.40 O SF22 Konishi USP 5739957 	Typically, 0.5–0.8
(e) 'P(P0)N' 	40×/1.20 W SF23 Okuyama USP 2003-0043473 	Corresponding to (a)(b)(c)(d)
(f) '(P0)PN' 	20×/0.90 W SF18 Nobis USP 9696536 	Corresponding to (a)(b)(c)(d)
(g) 'P(POP)N' 	60×/0.70 LD SF18 Shimizu USP 4666256 	Corresponding to (a)(b)(c)(d)

Based on the structural behaviour and the aberration correction strategies, the functionality of the two or three groups can be summarised. In Sections 4–6, the respective lens modules in each group are analysed.

– **The front group**, with great positive optical power, consists of several quasi-aplanatic meniscus lenses. It helps the system collect a large aperture angle. However, in the practical systems, the aplanatic condition

cannot be perfectly fulfilled. Typically, the first lens is designed to be hemispherical with a high refractive index to further increase the NA without introducing tremendous SA. There is residual SA, coma, FC, ACA and LCA, which should be compensated by the following groups. However, the FC can be reduced by an embedded front lens structure.

- **The middle group** (rear group in the two-group systems), which is composed of several cemented doublets and triplets, provides great contribution to SA (including zonal error), coma and ACA correction. Combining the ACA and SA, the higher-order induced spherochromatism should also be corrected in the middle group. In most of the sophisticated systems, the middle group consists of 6–10 elements with different cementing configurations. Although the positive middle group can correct the most crucial aberrations, as a drawback, it always generates a negative Petzval curvature and it usually slightly introduces astigmatism in the systems with larger etendue.
- **The rear group** is usually designed with negative optical power or weak optical power for FC correction. In order to correct the residual error from the front and middle group, thick meniscus lenses are often utilised, thus generating a positive Petzval curvature. The thick meniscus lenses may have quasi-symmetric and cemented structures in order to flatten the field for several colours. The residual astigmatism can also be corrected by this structure. In the low etendue system, it often significantly contributes to coma correction, while in the high etendue systems, it reduces the contribution for coma compensation and turns to SA correction. The thick lenses and cemented meniscus lenses can also be introduced into the rear group to further correct or control the lateral chromatic aberration.

### 3 Optical power distribution and general material selection

According to the overview of aberrations, the functionality of each lens group in the SA, coma and FC correction mostly depends on the optical power distribution of the system. Prior to the analysis of the detailed lens modules in each lens group, the basic optical power distribution is introduced in this section. The general consideration of the material selection for the ACA correction is also introduced.

#### 3.1 Optical power distribution

Among the six zones of the microscope objective classification based on etendue, the optical power distribution has four basic types:

1. Double-Gauss objectives in Zones 1 and 2.
2. Zones 1–4: basic optical power distribution with the positive front group, the positive middle group and the negative rear group and the ‘PPN’ structure as an overall retrofocus type system. Concerning the relative marginal ray height in each group, this type could be further classified. Moreover, corresponding to different correction strategies, the total power of the rear group could be designed so that it is very small and almost approaching zero. There are various power distribution types of the optical elements in the compound middle group, which is highly influenced by the application.
3. Zone 5: very-low-magnification objective with the positive front group, the negative middle group and the positive rear group and the PNP structure.
4. Zone 6: very-high-magnification long working distance objective with the positive front group, positive middle group and negative rear group and PPN strong retrofocus structure.

Owing to the applications, the optical power distributions of the Zone 5 and Zone 6 systems are different from the basic Zones 1–4 systems, which shall be discussed in Part III. When it comes to the double-Gauss system, the basic correction principle is well known, which is adopted from the classical photographic objective design. The coma is well controlled by the quasi-symmetric structure and the FC is corrected by the two meniscus cemented lenses. However, this structure typically cannot efficiently correct the SA introduced by NA larger than 0.5. Therefore, it could only be used to extend the working distance of the low NA systems with low/medium etendue, which are found in Zones 1 and 2. According to the classical theorem, to correct the symmetric aberrations (coma, distortion and lateral colour) the aperture stop of the double-Gauss objective should locate in the middle of the system in order to realise the symmetric chief ray path. Nevertheless, in the double-Gauss type microscope objective, since its back focal plane is typically located behind the system, this feature cannot be implemented due to the requirement of a telecentric object space. To move the focal plane towards the front part, some patented systems, e.g. system (A) in Figure 6, adds the front quasi-aplanatic shell-lenses with strong optical power, which also effectively collects the high NA. On the contrary, if an

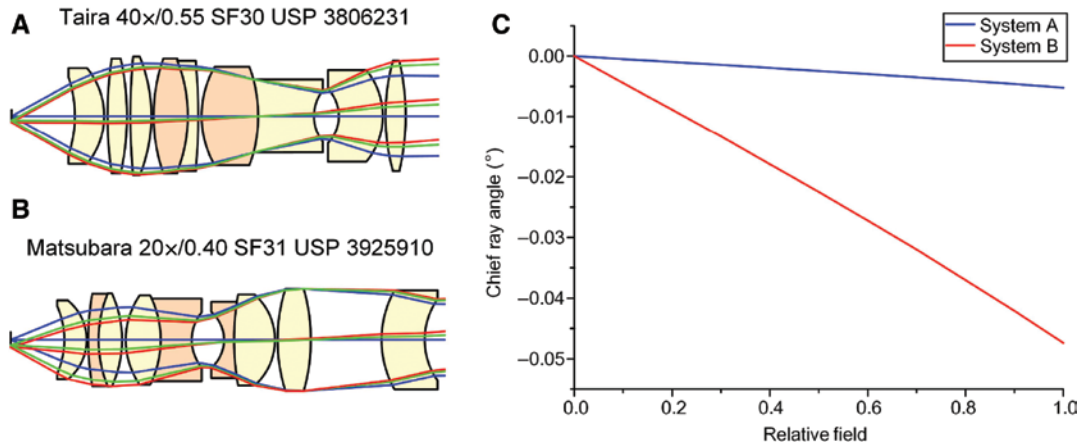


**Figure 6:** (A) Double-Gauss type microscope objective with compound front group. The back focal plane is shifted towards the front part of the system. (B) Double-Gauss type microscope objective with additional rear group. The back focal plane locates at the rear part of the system. (C) Object space telecentricity of system A and system B, which is measured by the object space chief ray angle.

additional rear group is inserted to compensate the FC, the back focal plane is moved towards the rear part, and thereby the telecentricity and excellent symmetric aberration correction cannot be realised simultaneously. In the example system (B), the aperture stop is set between the best-telecentric-position and the best-correction-position. Compared with system (A), the telecentricity is hampered. In the practical double-Gauss type objective, the aperture stop is not set to perfectly fulfil the symmetry principle, but the quasi-symmetric structure still effectively restrains the coma. A similar idea is also adopted by the Gauss-type rear group, which shall be introduced in Section 6.2.

The optical power distribution of most Zones 1–4 systems could be generally understood as the PPN retrofocus structure shown in Figure 7, which is widely used to extend working distance. The retrofocus system is conventionally characterised by a ratio between the working distance and effective focal length. However, as introduced in Section 4.3.1 of Part I, the working distance of the microscope objective is not only dependent on the optical structure, but is also significantly influenced by the

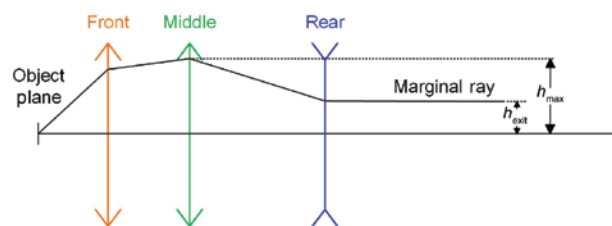


**Figure 7:** PPN retrofocus structure of most Zones 1–4 microscope objectives.

environmental condition and application requests. Therefore, a retrofocus factor  $r$ , which is defined in Equation (3) as the ratio between the maximum marginal ray height in the middle group ( $h_{\text{max}}$ ) and the marginal ray height of the exit ray bundle ( $h_{\text{exit}}$ ), is utilised as a measure to quantitatively classify the various practical retrofocus-like optical power distributions. The majority of collected systems have the PPN structure with the retrofocus factor  $r$  ranging between 0.25 and 0.8. To further extend the working distance, the retrofocus factor should be reduced. We name the PPN objectives with retrofocus factor below 0.25 as ‘PPN strong retrofocus’ to show its extraordinary retrofocus effect. With increasing etendue, the  $h_{\text{exit}}$  is extended and could even be larger than the  $h_{\text{max}}$ . Although the corresponding system may not have the retrofocus effect, they can be characterised by this factor larger than 0.8.

$$r = \frac{h_{\text{exit}}}{h_{\text{max}}} \quad (3)$$

According to the retrofocus factor and application requests, the various power distributions of Zones 1–4 systems can be classified into the following seven types. Concerning the objective corrected for infinite-conjugate, the basic structures of the optical power distribution types and the representative systems are shown in Table 2.

The type (a) PPN, which consists of a positive front group, a positive middle group and a negative rear group, is the most commonly used power distribution in the microscope objectives with medium and high magnification. The positive middle group mainly corrects the ACA introduced by the front group, but generates large residual SA, which should be compensated by the

negative rear group with large marginal ray height. The negative power of the rear group is also beneficial to the FC compensation. Furthermore, given that the chief ray height in the rear group is also high, associated with the large marginal ray height and great power, the rear group contributes significantly to coma correction.

The type (b) PPN strong retrofocus also consists of a positive front group, a positive middle group and a negative rear group, but it is typically used in high magnification objectives with long working distance. According to the retrofocus principle, to enlarge working distance, the rear group is designed with great negative power and low marginal ray height, while the middle and front groups are designed with strong positive power and large marginal ray height. Therefore, the rear group typically has a very small contribution to SA and coma compensation. However, due to its negative power and special material selection, it still has the functionality of FC and lateral colour correction. However, as the rear group does not compensate SA and coma, the complexity of the middle group typically increases to correct the SA, coma and ACA simultaneously.

The general power distribution of the type (c) is still PPN, if we consider the optical power of the entire rear group. However, as this type is used for objectives with low magnification and high NA (extreme etendue), due to the enlarged exit pupil size, the marginal ray height at the exit of rear group should be larger than its height in the middle group. Consequently, the rear group is designed with weak negative power and quasi-symmetric structure, which consists of a negative sub-group and another positive sub-group forming the magnification of rear group larger than 1. This structure is helpful in fulfilling the condition of FC correction and avoiding the generation of a higher-order coma. Typically, although the overall power is small, this rear group has large contribution to SA correction owing to the large marginal ray height.

Type (d) adopts a similar idea to Type (c) by designing the rear group with weak negative power or afocal. To realise this power distribution, the middle group should have a strong positive sub-group and another strong negative sub-group. Thereby, concerning the infinite-conjugate objective, the infinity space can be almost achieved between the middle and rear group. Consequently, the afocal rear group can be designed so that it is nearly free of SA. As the marginal ray height is large, if a single or cemented meniscus lens is used, it could contribute significantly to coma compensation. If a quasi-symmetric structure is utilised, the rear group could also be designed to be free of coma, thus leaving a great degree of freedom to compensate the FC and lateral colour.

Types (e) through (g) are applied to the microscope objectives with the CORR function. The modern CORR objectives utilise at least one movable group to compensate the tremendous SA induced by the change of cover glass thickness (CG), the type of immersion liquid, temperature and imaging depth [1]. However, as a major requirement, when the lens group is moved, the system's overall focal length cannot be changed significantly, and the chromatic correction cannot be violated. Consequently, the moving group is usually designed to be nearly afocal and free of ACA. To correct the SA, it is typically introduced in the front or middle group with large marginal ray height. In the type (e) example often used by Nikon, in order to adjust the CG thickness, a weak power cemented triplet, which well corrects the ACA, is inserted between the middle and rear group. The triplet is very sensitive to SA. When it comes to the type (f) example, the movable meniscus lens between the front and middle groups is designed with weak power to realise the depth adjustment for automatic Z-stack scanning. The element is made of glass with low dispersion in order to avoid hampering the chromatic correction. The type (g) example system utilised an afocal movable cemented triplet with low dispersion in the centre of the middle group. Compared with type (e) and type (f), the element is less sensitive to SA, but has a wider range of movement. Consequently, this structure could adjust the CG thickness with a larger range, which is widely used in the inverted microscope and semiconductor applications.

Notably, the special optical power distribution is only a fine adjustment within one individual group, whereas the overall power distribution like Types (a)–(d) can be applied depending on the system NA and magnification. For instance, the example systems for Types (e) and (f) have rear groups with weak power, similar to Type (d), and the overall power distribution of the example system for Type (g) is the typical PNP retrofocus type (b). Arranging the special power distribution is not the unique solution to realise CORR function in the modern microscope objectives. A systematic discussion of other approaches will be given in Part III.

In summary, owing to the characteristic of the microscope objective, the front and middle groups are always designed with positive power. Nevertheless, the power of the rear group can be significantly influenced by the magnification and correction strategy of the SA and coma. In order to extend the working distance, the double-Gauss structure is used for low NA, low/medium etendue systems, while the PPN strong retrofocus type is utilised for high NA, medium etendue systems. Furthermore, highly influenced by the requirement of

CORR function from applications, the power distribution of the sub-groups within the front and middle group can be finely adjusted.

### 3.2 General material selection strategy

The selection of materials is the second most important factor influencing the functionality of lens modules for aberration correction, particularly for the chromatic aberration correction. In this section, the following four general considerations of material selection are introduced (the concrete glass selection will be demonstrated in Sections 4–6 with a detailed discussion on lens modules):

1. Transmittance;
2. Refractive index and dispersion;
3. Relative dispersion for secondary spectrum correction, including the extended spectral range; and
4. Autofluorescence and manufacturing consideration.

As the most classical and common method to sort optical materials, particularly for optical glasses, the Abbe diagram for the d-line is shown in Figure 8, where the glass labels from three often used vendors (Schott, Ohara and Hoya) are marked in the corresponding zones. Some important glass types with specific advantages for the four considerations are pointed out, and these shall be discussed later in detail. The ‘Middle Glasses’ are defined by the Abbe numbers between 50 and 57, whereas the ‘KZFS Short Flint’ gives the region of the short flint glasses with the glass label of KZFS or KZFH.

The transmittance of the optical material is the most basic consideration for material selection in the refractive optical system. Figure 9 demonstrates the transmittance of the 438 glasses from the three glass vendors, which is measured with a 10 mm glass sample under the respective wavelengths of 2000, 1000, 400, 360 and 340 nm. The specified wavelengths cover the spectral range of typical microscope objectives from UV to IR.

Concerning the conventional microscope objectives corrected for visible spectrum, with the exception of some SF glasses with high refractive index, which have low transmittance in blue, most of the optical glasses and crystals can be used and these have excellent transmittance (>90% for a 10 mm sample) ranging from about 400–1000 nm. However, the number of selectable materials is reduced when the working wavelength is extended to the UV and IR range, which is useful for fluorescence microscopy and semiconductor inspection application.

Regarding the extension to the IR side, despite the non-eco-friendly effect, some old glasses with lead have good UV transmission at 360 nm, but they are not transparent in NIR. In the later developed lead-free solution, their IR transmittances are improved. According to Figure 9, most of the glasses have excellent transmittance at 2000 nm, while 117 old glasses have zero transmittance. Therefore, in the current development of IR-capable objectives, the selection of material is not critical concerning transmittance.

When it comes to UV extension, the 340 and 360 nm wavelengths are usually required for epi-fluorescence excitation, whereas the 3rd harmonic wave 355 nm of

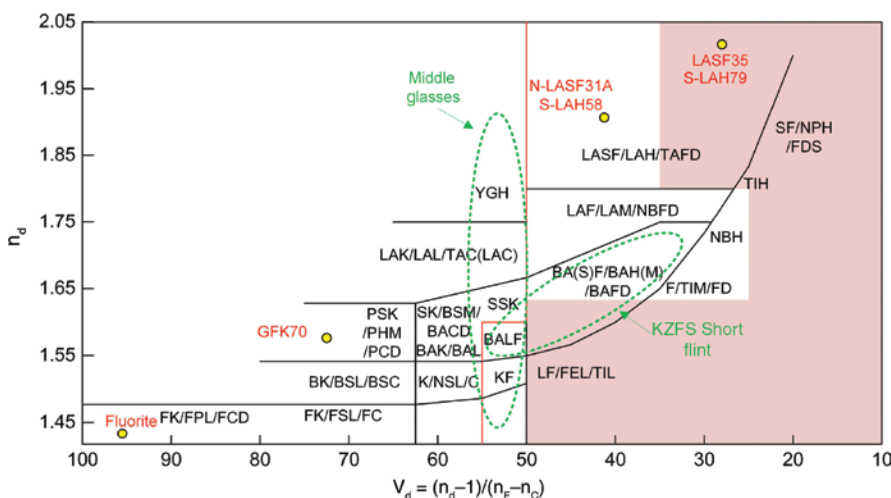


**Figure 8:** Abbe diagram with the glass labels from three often used vendors. The red line separates the crown and flint glasses and the red area indicates the forbidden zone of material selection for high-contrast fluorescence imaging. The green encircled areas demonstrate the region of Middle Glasses and KZFS Short Flint.

the YAG laser is used for semiconductor inspection. To ensure adequate excitation intensity on the specimen, at least 60%–80% transmittance of the entire lens system is required [12]. Consequently, glasses with at least 80%–90% transmittance (10 mm sample) at 340 and 360 nm should be selected and thick elements should be avoided. According to Figure 9, less than 25% of the glasses can be used for the UV-capable objectives, which mostly belong to the FK, BK, PSK types, the Middle Glasses and the KZFS Short Flints. It should also be noted that UV transmission is important for microlithography applications, under which circumstance the working spectrum is nearly monochromatic in DUV, such as 248 and 193 nm. Although some FK glasses still have excellent transmission at around 320 nm, below 300 nm, none of the glasses are selectable. Typically, only fused silica, which exhibits 98% transmission down to 193 nm, and fluorite, which has transmittance over 99% at 157 nm, could be utilised for the DUV application. This special case is excluded from our discussion.

The second and third considerations are associated with the correction of the spherical and chromatic aberrations. The basic principles of achromatism and SA correction are well known. However, according to the discussion in Sections 2.2 and 3.1, compared with the classical Achromate, due to the greater burden of correction, the design of microscope objective prefers using compensation between different groups instead of perfect correction within individual elements. In practice, the overall chromatic aberration is balanced by several cemented components. Similar to classical Achromate, in the positive cemented doublets, the positive component is made of low dispersive crown glass, whereas the negative component

is made of flint glass with large dispersion. The materials of each cemented element should be selected with large difference of Abbe number (ratio) and relatively small index gap ( $<0.3$ ). Thereby, the arbitrary chromatic aberration contribution could be generated by appropriate power distribution of the two components, while the bending of the cemented surface is relaxed to avoid critical sensitivity.

The utilisation of optical materials with large refractive index can relax the surface bending to achieve greater optical power with less SA. Particularly, concerning the front group, if the aplanatic lenses are made of high-index materials, the large object NA could be collected more efficiently, thus relaxing the correction burden of the middle group. However, according to Figure 8, materials with extremely large refractive index typically suffer from critical dispersion (Abbe number  $v < 30$ ), which would introduce tremendous chromatic aberration under great optical power. To reduce this large contribution, optical materials towards the top-left on the Abbe diagram are preferred. Therefore, in high NA systems, the N-LASF31A or L-LAH58 are typically used instead of LASF35 or L-LAH79 as the front lens, whereas the GFK70 is preferred in the medium NA systems. A combination of these two glasses is also widely used. Generally speaking, materials with a large refractive index and less dispersion are preferred. Consequently, the LAK, LAF and LASF glasses are better choices compared with the SF glasses used in the conventional Achromate.

When the corrected spectrum is extended, in order to correct the secondary spectrum and higher-order ACA, the partial dispersion should be considered. Concerning the typical Apochromate with class (c) correction defined in Part I, the partial dispersion of the g-line should be considered. Typically, the relative partial dispersion of the g-line is specified as  $P_{gF} = (n_g - n_F) / (n_F - n_C)$ , which can be sorted versus the Abbe number, shown as Figure 10.

According to the apochromatism theorem, when the achromatism is realised, if the partial dispersion of the optical components is identical, the secondary spectrum is eliminated, thereby forming two saddle points on the chromatic focal shift curve in the green region and the violet region, respectively. Therefore, in the conventional Apochromate, such as a cemented triplet, three materials forming a large area on the partial dispersion diagram are selected, including the anomalous dispersive fluor crown (FK/FPL) or fluorite, short flint and SF glasses [13]. However, when it comes to the design of the microscope objectives, typically, the SF glasses with large dispersion are not used in the middle group for ACA correction. The g-line and F-line partial dispersion of the selected

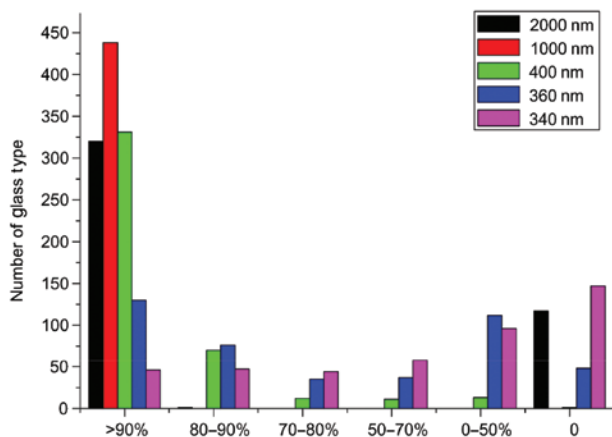


**Figure 9:** Number of glasses with six levels of transmittance at five specific wavelengths from UV to IR, which is measured with a 10 mm-thick glass sample.

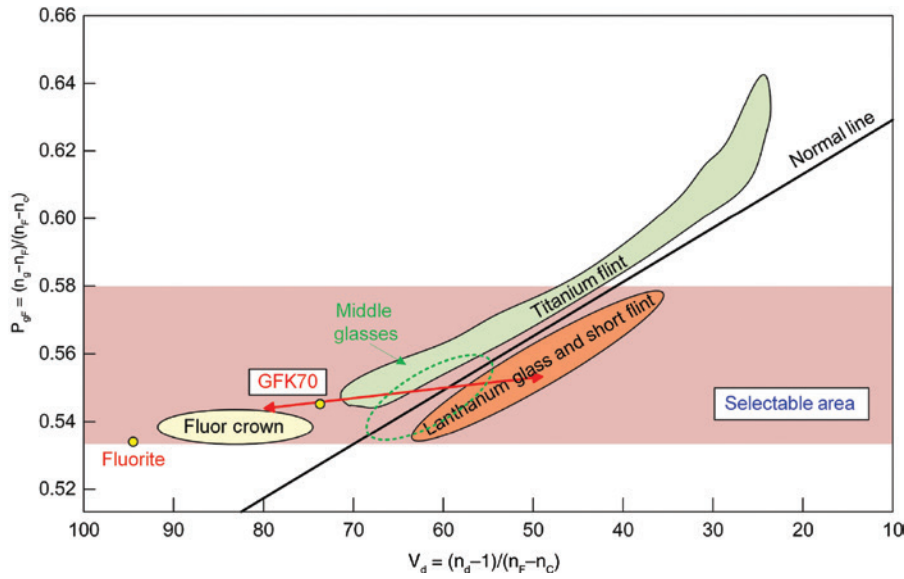


Figure 10: Partial dispersion diagram for the g-line and F-line. The normal line is defined by the K7 and F2 glasses (Schott convention).

materials mostly lie in the range between 0.535 and 0.58 (the optimal area is within 0.535–0.56). All the favourable glasses for the transmittance consideration and achromatism consideration are included within this range. By selecting materials from this narrowed region, the optical power of the components could be relaxed to correct the secondary spectrum.

When the corrected spectrum is extended, the two saddle points on the chromatic focal shift curve should be shifted to UV and IR in order to realise

super-apochromatism. The partial dispersion of the extended wavelength should also be considered. The partial dispersions of all the Schott glasses are plotted in Figure 11 with both the  $P_{gF}$  and  $P_{Cs}$ .

According to Figure 11, the fluor crown and short flint have anomalous partial dispersion in both the blue side (g-F) and the red side (C-s), while the Middle Glasses have normal dispersion in both sides. On the contrary, the SF only has anomalous dispersion on blue side. Therefore, typically utilising the glasses in the selectable

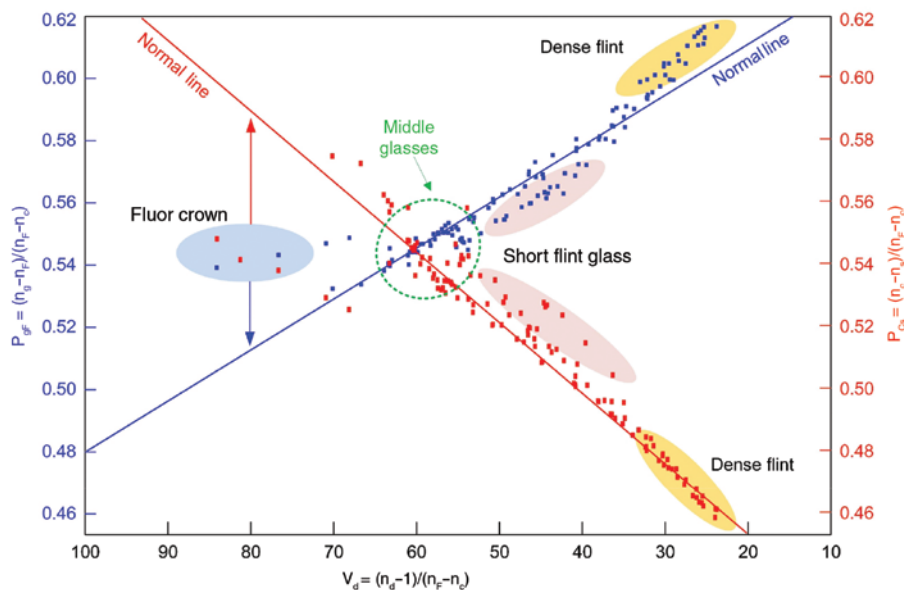


Figure 11: Partial dispersion diagram for both the g-F-line and C-s-line of the Schott glasses. The normal line is defined by the K7 and F2 glasses.

area shown in Figure 10 could also correct the secondary spectrum for extended spectral range, but the SF glasses cannot be used.

The last aspect is typically less considered. Only in the microscope objective for high-contrast epi-fluorescence imaging, the reduction of autofluorescence is important. Materials containing  $\text{Nb}_2\text{O}_5$  or  $\text{Ta}_2\text{O}_5$  as constituents, e.g. NBH-class from Ohara, are widely used because of the advantageous features of excellent UV and VIS transmittance and low autofluorescence. According to the patents [14–18], materials cannot be selected from the forbidden zone, which is marked on the Abbe diagram in Figure 8. The materials with large dispersion typically induce great autofluorescence under high illumination intensity. Notably, most of the materials with extremely high refractive index cannot be used. Despite the consideration of introducing less chromatic aberration, this is also a reason why the high index materials with relatively low dispersion, such as N-LASF31A, are popular choice to be used in the front group of high NA systems. More details associated with lens structure will be introduced in Section 4. The material selection sometime also depends on the element fabrication and system assembly consideration to reduce cost or improve system robustness. For instance, the glasses with the d-line refractive index larger than 1.8 are typically hard. Consequently, if it is used for the front lens, it is difficult and time-consuming to polish the front concave surface precisely, which should be avoided in the cost-driven design [19].

As a conclusion, according to the four considerations, based on the philosophy of aberration compensation by different groups, the materials with anomalous dispersion and the materials with medium refractive index and medium dispersion are widely used in the modern microscope objectives with high performance. Generally speaking, glasses from the FPL, YGH and NBH series of Ohara; the LAK, LASF and KZFS series of Schott and the GFK series of Sumita are selected by most of the vendors.

## 4 Lens modules in the front group

According to the aberration correction strategy discussed in Sections 2 and 3, each of the microscope objectives from Zones 1–4 can be divided into two or three functional group. From this section, the lens modules utilised in each group are discussed in detail. The major function of the front group is to collect the large object NA and suppress the introduced SA and ACA. In order to collect the large aperture without introducing much SA,

the aplanatic condition is effectively utilised. To restrain the introduced chromatic aberration and relax the correction burden of the middle group, the material should be carefully selected. In order to fulfil the requirement from modern biomedical applications, various special structure and new techniques are also applied to the front group. Concerning these three aspects, the functionalities of the lens modules used in the front group are systematically analysed with respect to aberration correction, application and system manufacture. However, the detailed mechanical realisation of the front group is less discussed, which is recently well described by Frolov et al. [20].

### 4.1 Aplanatic lenses

The basic aplanatic principle for the spherical-aberration-free imaging is well known [13]. Utilising several quasi-aplanatic lenses, a design approach has been introduced to synthesise the front group of the microscope objective [21]. According to Equation (1), the SA vanishes under three conditions ( $H=0$ ,  $I'=I$ ,  $I'=U$ ), which correspond to the following three cases: the marginal ray has zero height at the surface, the marginal ray has no refraction on the surface and the marginal ray fulfils aplanatic condition. The three cases are named as vertex, concentric and aplanatic, respectively. Fulfilling these three conditions, the surface can generate an image that is free of all orders of the SA and linear coma. Combining two of these conditions, three lens setups are widely used in the front group of the microscope objectives as shown in Figure 12.

The type (A) v-c lens has the shape of hemisphere, while the type (B) v-a lens – the famous Amici lens – is a hyper-hemisphere. The free working distance under these two cases is zero. To extend the working distance, the type (C) c-a meniscus lens is preferred. According to the object and image distance shown in Figure 12, the respective

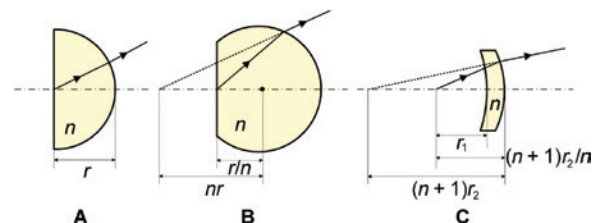


**Figure 12:** Typical aplanatic lenses with refractive index  $n$ . (A) vertex-concentric (v-c). (B) vertex-aplanatic (v-a). (C) concentric-aplanatic (c-a).



magnifications of these three aplanatic lenses can be calculated as follows:

$$\begin{aligned} M_{v-c} &= \frac{r}{r/n} = n, \quad M_{v-a} = \frac{(n+1)r}{(n+1)r/n^2} = n^2, \\ M_{c-a} &= \frac{(n+1)(2n-1)r_2^2 - 2n^2r_1r_2}{nr_1(r_2 - r_1)}. \end{aligned} \quad (4)$$

The v-c lens, which is typically used as a contact magnifier, has the same magnification as its refractive index. The concentric principle is also applied in the embedded front lens for immersion objective, which will be introduced in Section 4.3. The v-a Amici lens has an important functionality, that is, the magnification of the lens is the square of its refractive index, which means the large NA from the object could be lowered down with a factor of  $n^2$  after the aplanatic lens. Hence, the v-a lens, which is typically made of a high-index material, is typically used as the front lens of microscope objective and significantly reduces the complexity of following groups for aberration correction. When the Amici introduced the v-a lens made of flint glass ( $n=1.6-2.0$ ) into the old Lister or Petzval objective with NA of 0.2–0.3, the NA was enlarged by 2.5–4 times, resulting in approximately 0.65 for the dry lens and 1.2 for the oil immersion lens. However, according to Section 6 in Part I, the v-a lens has a major drawback in terms of system assembly under high NA, that is, the hyper-hemispherical lens cannot be mounted to the leading edge of the objective. When the type (C) c-a lens is applied, the working distance can be enlarged, which is identical to the radius of the front surface. However, for typical cases,  $M_{c-a} < M_{v-a}$ , the NA collection is less effective.

In practical systems, there are popular setups introducing the quasi-concentric-aplanatic shell-lenses into the front group to overcome the drawback of single v-a lens and c-a lens, which are shown in Figure 13. Solution (A) utilises a series of c-a lens to realise the high NA with sufficient free working distance. The strong power for NA collection is well distributed to the shell lenses. Thus, the decentring sensitivity of each element also reduces compared with a single element. This setup is typically used in the medium/high NA objectives with large magnification and long working distance, particularly for semiconductor inspection application. The rest of the high NA systems with short working distance mostly use the solution (B), which is a combination of the c-a shell-lenses and the v-a lens. Therefore, the high NA is effectively collected, whereas the hyper-hemispherical shape can be avoided under high NA. Notably, the SA is very sensitive to the axial shift of the meniscus elements in the shell-lens group. Corresponding to the power distribution type (f) in

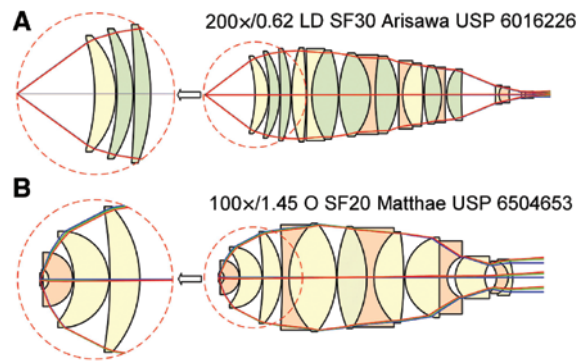


**Figure 13:** Practical front group with aplanatic shell-lenses (A) purely concentric-aplanatic shell-lenses. (B) vertex-aplanatic lens associated with concentric-aplanatic shell-lenses.

Table 2, by reducing its optical power, which might slightly violate the aplanatic condition, it is possible to realise the depth CORR by moving the meniscus lens.

Notably, for the dry objectives with extremely high NA, e.g.  $NA=0.95$ , the front surface must be designed so that it is concave in order to achieve sufficient free working distance; however, this cannot fulfil the aplanatic condition. Therefore, the ray bending on the front surface is usually large, which introduces tremendous SA. As a consequence, the special lens modules must be used in the middle group for compensation, particularly concerning higher-order SA. However, the thick meniscus front lens can generate a positive Petzval curvature with positive optical power, which relaxes the rear group for FC compensation. A detailed discussion will be given in Section 4.3.

## 4.2 Material selection

If the front lenses are made of optical material with higher refractive index ( $n_d > 1.90$ ), the front group can collect larger NA with the same bending, which could relax the middle group design and avoid hyper-hemisphere. Only a limited number of SF or Lanthanum SF glasses (LASF) can reach this high refractive index. According to Section 3.2, SF glasses are not preferred in the modern high-performance microscope objective, due to the limited transmittance and capability of chromatic correction. Furthermore, these glasses typically have poor stability and manufacturability. Consequently, the LASF glasses with excellent stability and superb transparency in blue are commonly selected for the front aplanatic lens. The most popular candidates are LASF35 ( $n_d=2.022$ ,  $v_d=29.06$ ) from Schott and S-LAH79 ( $n_d=2.003$ ,  $v_d=28.27$ )

from Ohara. However, due to the large dispersion, the aplanatic lens made of these LASF glasses would introduce tremendous chromatic aberration. To reduce this effect, first, as introduced in Section 3.2, the materials with medium refractive index ( $n_d=1.60\text{--}1.90$ ) and medium dispersion ( $v_d=40\text{--}60$ ) are preferred. Second, based on the front group structure consisting of vertex-aplanatic lens and followed shell-lenses, it is possible to design the shell-lenses with materials with low refractive index and low dispersion. Typically, these two methods could also be used together. Figure 14 demonstrates a comparison of two  $100\times/1.45$  oil immersion objectives with nearly equivalent performance. The front lenses are designed to be quasi-vertex-aplanatic with an embedded structure, which shall be discussed in Section 4.3. However, concerning the material selection, the system (A) from Carl Zeiss utilised both two methods, selecting medium-index, medium dispersive glass N-LASF31 ( $n_d=1.881$ ,  $v_d=41.01$ ) in the front aplanatic embedded lens, followed by two shell-lenses made of low-index, low dispersive glass N-FK51 ( $n_d=1.487$ ,  $v_d=84.47$ ) and N-PK51 ( $n_d=1.529$ ,  $v_d=76.98$ ), while the system (B) from Nikon only used the second method, selecting S-LAH79 for the front lens and producing the shell lens with medium-index, low dispersive material K-GFK68 ( $n_d=1.592$ ,  $v_d=68.37$ ). Consequently, the system (B) requires more elements in the middle group to correct the larger residual chromatic aberration.

If we change the high-index LASF glass in system (B) to N-LASF31A or S-LAH59 instead of S-LAH79, the resulting front group structure is the most popular solution for high NA objective design. Taking the advantage of the relatively high refractive index and relatively low dispersion of these medium-index LASF and the following GFK70

( $n_d=1.569$ ,  $v_d=68.37$ ) or GFK68 from Sumita, the high NA could be efficiently collected without introducing tremendous chromatic aberration.

When it comes to the high-contrast fluorescence microscopy, concerning the common epi-fluorescence setup, the excitation light enters the objective from the rear part and reaches the highest intensity at the front group, where it is easy to generate autofluorescence [22]. Therefore, the materials used in the front group should be especially selected with low fluorescence efficiency. Marked as the forbidden zone in Figure 8, the high dispersive glasses with Abbe number  $v_d$  lower than 35 and Abbe number  $v_d$  lower than 50 together with d-line refractive index lower than 1.62 typically have large autofluorescence efficiency. However, the materials fulfilling the conditions of  $25 \leq v_d \leq 41$  and  $1.65 \leq n_d \leq 1.80$  have low autofluorescence and can be used for the high-contrast fluorescence imaging. To match this requirement, the high-index LASF glasses cannot be used, whereas the medium-index LASF glasses, such as N-LASF31A, are favourable. However, for some systems with high NA and high etendue used for fluorescence microscopy, it is necessary to use the high-index material to relax the complexity of the middle group. Therefore, special crystals with extremely high refractive index and low autofluorescence have been developed, e.g.  $\text{LiTaO}_3$  ( $n_d=2.187$ ,  $v_d=23.9$ ). However, they are only used in a limited number of special products [23].

In summary, to effectively collect the high NA, materials with high refractive index are preferred in the front group. However, to reduce the introduced chromatic aberration and autofluorescence, the medium-index LASF glasses are widely used instead of the high-index LASF glasses. Furthermore, the low dispersive material with relatively high refractive index, particularly GFK glasses from Sumita and PK glasses from Scott, are useful in the shell-lenses to restrain chromatic aberration.

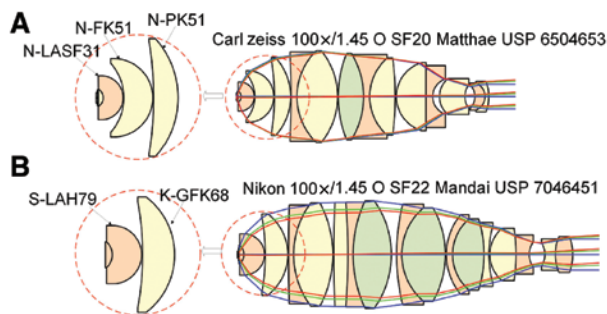


**Figure 14:**  $100\times/1.45$  oil immersion objectives with different material selection in the front group. (A) N-LASF31 is utilised with the embedded front lens made of N-BK7, which refractive index is nearly matched to the immersion oil. (B) S-LAH79 is utilised with the embedded front lens made of another flint glass KF6, whose refractive index is nearly matched to the immersion oil.

### 4.3 Embedded front lens and special techniques

In the immersion microscope objectives, the front lens is usually designed as an embedded structure consisting of a front small plano-convex lens and a rear large meniscus. The layout is shown as Figure 15. This front lens setup has great advantage in aberration correction, and its structure also matches the requirements from application.

In the objectives with immersion, the immersion liquid is used between the objective front surface and the specimen (or cover glass). If the front surface of

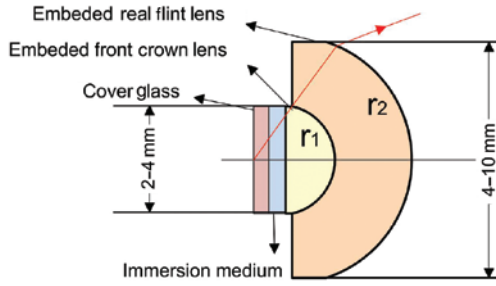


**Figure 15:** Embedded front lens in high NA immersion microscope objectives. The front embedded crown plano-convex lens typically has diameter between 2 mm and 4 mm, while the rear flint meniscus lens has clear diameter between 4 mm and 10 mm. With special technology, the diameter of the front lens could reach a minimum value around 1.1 mm. The radius of the cementing surface is  $r_1$  and the radius of the rear surface is  $r_2$ . The refractive indices of the two components are  $n_1$  and  $n_2$ , respectively.

the front lens has a strong curvature, which is typically used in the high NA dry objective, this can lead to the generation of air bubbles on the surface during observation. It is also difficult to clean the front surface when the observation is finished or when the specimen is changed. Therefore, the front surface in most immersion objectives is designed as a plane, only with few exceptions [24], in which the front surface is slightly curved with removable bubble.

According to Section 4.2, optical materials with high or medium refractive index are usually selected for the front lens. However, when the high-index material is used, the planar front surface would bring up two critical problems in system design. For one thing, similar to the discussion of cover glass in Section 4.3.2 of Part I, as the refractive index of the front lens and the immersion medium are not matched, the planar surface could generate large amount of SA. For another, when the epi-illumination setup is utilised, total internal reflection (TIR) may occur at the planar front surface. For instance, assuming the front lens is made of LASF35 with d-line index of 2.022, whereas the d-line immersion liquid index is 1.515 (Type A) for oil immersion and 1.333 for water immersion, the large index gap of over 0.3 would induce tremendous SA. The maximum NA limited by TIR for the two immersion cases are respectively given by

$$NA_{\text{oil}} = n_{\text{oil}} \cdot \sin \theta_{\text{c-oil}} = 1.515 \cdot \frac{1.515}{2.022} = 1.135, \quad (5)$$

$$NA_{\text{water}} = n_{\text{water}} \cdot \sin \theta_{\text{c-water}} = 1.333 \cdot \frac{1.333}{2.022} = 0.879, \quad (6)$$

which means the front planar LASF35 lens cannot be used for objectives with NA larger than 1.135 and 0.879 for oil and water immersion, respectively. Therefore, the embedded lens with a low index material, which has matched refractive index to the immersion liquid, is utilised for high NA immersion objectives.

To fabricate the embedded lens with two parts, due to the small size and radius, special techniques, such as ball technology, should be applied. Given that the front surface is a plane, the difficulty of surface processing is reduced. However, to realise the accurate processing of the cemented surface, the material should be carefully selected. Table 3 summarises the commonly used materials for the plano-convex lens.

All of the simple materials in Table 3 are easy to machine in order to form the very small surface radius with high accuracy. Under the circumstance of oil immersion, the refractive indices of the cover glass, immersion liquid and the front embedded lens are almost perfectly matched. Therefore, the cementing surface can be designed to be concentric with the object, so that the SA is not generated at the cemented surface with large index gap. Consequently, the SA is reduced, and a higher NA can be achieved. As illustrated in Section 4.3.1 of Part I, given that the cementing surface is concentric, under a certain NA, the free working distance lies around a nominal value. In high NA oil immersion systems, the free working distance is slightly enlarged compared with the natural value. However, when it comes to the water immersion, none of the available lens materials have a refractive index of around 1.333. Although the utilisation of FK5 glass and quartz could avoid TIR, there is still an index gap of around 0.1 between the optical material and the water. To compensate the induced SA, the curvature of the cemented surface and the rear surface should be adapted, thereby violating the aplanatic condition. To avoid this effect, some special systems slightly bend the front surface [24]; however, the cost increases to produce the tiny meniscus lens.

**Table 3:** Low refractive index glasses selected for the embedded front lens.

Glass type	Refractive index ( $n_d$ )	Abbe number ( $v_d$ )	Immersion Liquid
N-K5	1.522	59.48	Oil
N-BK7	1.517	64.17	Oil
N-FK5	1.487	70.41	Water
Quartz	1.458	67.83	Water

When it comes to its functionality in the aberration correction, the embedded front lens also has great advantage in the FC restraint. According to Petzval's theorem, the Petzval curvature, represented as Equation (7), is always negative for the conventional front groups, which are composed of positive  $v$ -a lenses and thin meniscus  $c$ -a shell-lenses

$$\frac{1}{R_{\text{Ptz}}} = -n' \sum_k \frac{n'_k - n_k}{n'_k n_k r_k}. \quad (7)$$

The embedded front lens should be designed with index-matched material, which is typically a low index crown, and the rear large meniscus lens should be designed with medium/high-index material (flint) to effectively collect NA. Therefore, based on the embedded lens structure shown in Figure 15, according to Equation (8), the overall Petzval curvature is usually positive, which is also true for the meniscus thick front lens in the dry objectives. Hence, the embedded front lens generates a positive Petzval curvature with great positive power, which could relax the complexity of rear group in the FC correction

$$\frac{1}{R_{\text{Ptz}}} = 0 - \frac{n_2 - n_1}{n_1 n_2 r_1} - \frac{1 - n_2}{n_2 r_2} = -\frac{1}{n_2} \left( \frac{n_2 - n_1}{n_1 r_1} + \frac{1 - n_2}{r_2} \right) > 0. \quad (8)$$

However, due to the special technology and high requirement of the manufacturing accuracy of the cemented surface, the embedded front lens is costly. Therefore, for cost-driven applications, a monolithic front lens is preferred. In the oil immersion objective, the monolithic front lens is made of a glass with nearly identical refractive index to the immersion oil. Therefore, the TIR is avoided for epi-illumination and the light is not refracted at the planar surface, which is beneficial to restrain SA. Owing to the low dispersion, the introduced chromatic aberration is also reduced. However, due to the low refractive index, a high NA cannot be effectively collected. As the limit of a hemispherical lens shape is reached, only a small NA = 1.25 can be realised.

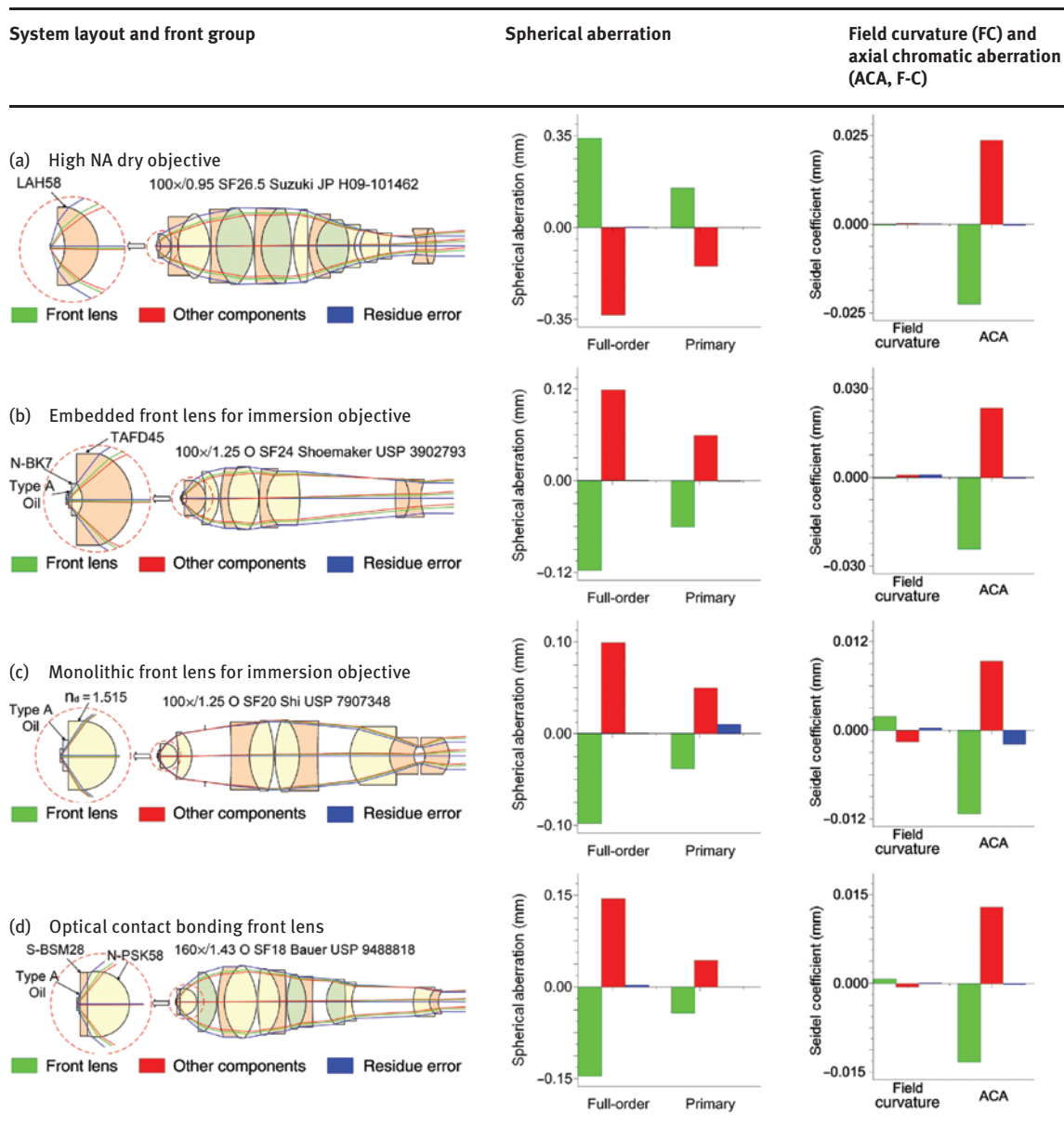
In the latest development of super-resolution localization microscopy, stronger laser power is utilised for photo-activation. Due to the high energy intensity in the front lens with high numerical aperture, the cementing glue can be easily damaged, particularly under UV excitation. Furthermore, the adhesion has a specific autofluorescence, which would reduce the contrast of the fluorescing sample. As a glueless technique, the 'optical contact bonding' becomes a feasible solution to manufacture the front cemented lens [25]. To realise the

bonding with intermolecular force, the contact surface must be conformal to an accuracy of better than 1 nm. Thus, planar contact surface is preferred. However, for the immersion objective with epi-illumination, to avoid TIR, the refractive index of the front lens material cannot be selected too large. As an example, the system (d) in Table 4 utilised the method with bonding of S-BSM28 ( $n_d = 1.618$ ,  $v_d = 49.82$ ) and N-PSK58 ( $n_d = 1.569$ ,  $v_d = 71.21$ ) glasses. NA = 1.43 is achievable without TIR and the utilisation of low dispersive PSK glass can restrain the introduced chromatic aberration. However, this positive front lens can only generate a negative Petzval curvature. Due to the low refractive index of N-PSK58, to restrain the SA, the quasi-vertex-aplanatic lens has hyper-hemispherical shape, which is difficult to mount. Nevertheless, according to the discussion in Section 6 of Part I, it is possible to mount the whole front lens on the S-BSM28 plane plate.

The functionalities of the aberration correction, the front lens of a high NA dry objective, the typical embedded front lens for the immersion objective, the monolithic front lens for immersion objective and the novel front lens utilising optical contact bonding technology are compared in Table 4 with practical examples.

The system (a) utilised a thick meniscus front lens made of LAH58 ( $n_d = 1.883$ ,  $v_d = 40.78$ ). Owing to its relatively high index and relatively low dispersion, the high NA = 0.95 is effectively obtained without tremendous ACA. The material also has relatively low autofluorescence efficiency to improve the contrast of fluorescence image. In order to realise the acceptable free working distance of 0.38 mm, the designed concave front surface cannot fulfil the aplanatic condition. Therefore, it generates a large positive SA with tremendous higher-order contribution, which is different from the slight negative SA generated by the other systems. However, because of the thick meniscus shape, according to Equation (6), the element is nearly free of the Petzval curvature. Consequently, the middle group of system (a) becomes very complicated as it compensates the SA, while the rear group becomes relatively simple due to the relaxation of the FC correction.

The systems (b)–(d) are immersion objectives with Type A oil as immersion liquid, which have been used as example in the Section 6 of Part I. The conventional embedded lens used in system (b) selected N-BK7 as the index-matched material and the high index TAFD45 ( $n_d = 1.954$ ,  $v_d = 32.32$ ) glass for the rear meniscus part. The front lens is quasi-aplanatic, introducing slight SA. The FC is also restrained by generating a slight positive Petzval curvature according to Equation (8). However,

**Table 4:** Comparison of the front lenses in practical microscope objectives.

due to the large dispersion of TAFD45, the introduced ACA is greater.

The system (c) used a monolithic v-a lens made of a glass with a d-line index of 1.515 and Abbe number about 61, which is matched to the immersion liquid. Taking advantage of the low dispersion, the introduced ACA is only half of the system (b) under identical NA. However, due to its low index, compared with system (b), the rear curvature has a greater bend, reaching the limit of hemisphere. Furthermore, the monolithic front lens generates tremendous negative Petzval curvature, which is then compensated by the ‘Gauss type’ rear group.






#### 4.4 Summary

According to the discussion from Sections 4.1 to 4.3, the ten lens modules utilised in the front group are summarised in Table 5 in terms of their functionality in restraining the three major aberrations: SA, FC and ACA. Furthermore, the relationship between the lens modules and system parameters (NA and working distance, WD) is illustrated and the special impacts of the application and considerations of manufacturing and technology are also marked. The number following the name of the lens modules indicates the number of the analysed systems.

**Table 5:** Summary of lens modules in the front group.

No.	Lens modules	Aberration restraint			System parameter		Application/manufacturing and technology considerations
		SA	FC	ACA	NA	W.D.	
1	Aplanatic v-a lens (243)	Coma		–			Hyper-hemisphere hard to mount
2	Aplanatic c-a lens (285)	Coma		–			–
3	Aplanatic shell-lenses (264)	Coma		–			Possible CORR
4	Thick meniscus front lens in dry objective (79)			–			–
5	High refractive index material (245)			–			Large autofluorescence
6	Medium refractive index material with medium Abbe number (130)			–			Low autofluorescence
7	Low refractive index material in shell-lenses (179)			–			Low autofluorescence
8	Embedded front lens with index-matched material (144)			–			Epi-illumination, immersion
9	Monolithic front lens with index-matched material (28)			–			Easy to produce, low cost, epi-illumination, immersion
10	Front lens with optical contact bonding (1)			–			Localisation microscopy, low autofluorescence, capable to mount hyper-hemisphere

	Great positive effect		Significant positive effect		Slight positive effect
	Slight negative effect		Significant negative effect	–	Negligible effect

It is notable that multiple lens modules could be used in the front group of an objective lens.

### 5 Lens modules in the middle group

The middle group plays a key role in correcting the SA and ACA, which are introduced by the front group. As a common layout, several cemented doublets and triplets constitute the positive middle group with relatively large optical power. According to Section 3.2, concerning the correction of the ACAs, including the secondary and higher-order spectra, the materials used in the cemented lenses are selected with distinct Abbe numbers but similar partial dispersions.

However, the correction of the aberrations mentioned above is not sufficient to improve the longitudinal polychromatic performance of the high NA system. To further improve the resolution and contrast of the image, the zonal SA (zonal error) and chromatic deviation of the SA, namely, spherochromatism, must be controlled. The longitudinal aberration of systems with different levels of zonal error and spherochromatism correction are compared in Figure 16.

The longitudinal aberration (A) represents the typical performance of the conventional Achromate objectives, where the ACAs of red and blue light are well corrected near the full aperture, but the residual

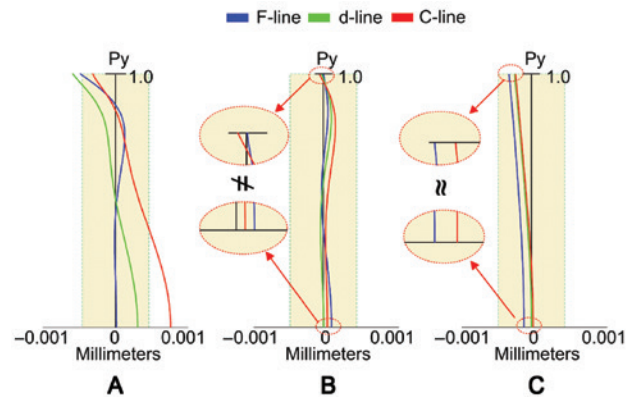


**Figure 16:** The longitudinal aberrations of different correction levels, where  $P_y$  is the relative pupil height and the shaded region indicates the depth of focus of d-line. The spherochromatism is measured by the difference between the red and blue light for paraxial case and full aperture. (A) Achromatic axial colour correction with spherochromatism correction of green and red light. (B) Apochromatic axial colour correction with certain ZSA and spherochromatism control. (C) Apochromatic correction with excellent spherochromatism and ZSA correction. The three systems correspond to the system (a), (c) and (d) with identical NA demonstrated in Table 2 of Part I. Only the F-line, d-line and C-line correction are compared, without g-line performance demonstration of the apochromatic systems.

secondary spectrum of the d-line exists. To control the longitudinal aberration of d-line, the spherochromatism of the d-line and the C-line is corrected, thus the

focal shift through the full spectrum is controlled within  $2.5 \times \text{DoF}$  (Depth of Field). When it comes to the Apochromate system (B), the ACA and secondary spectrum are perfectly corrected for the three colours near the boundary aperture. The SA of the d-line is also cancelled for centroid green light. However, concerning the zonal error and spherochromatism, although they are controlled within the DoF, but the performance at different zones are slightly different. The correction is not as perfect as the state-of-the-art system (C). Both the zonal error and the spherochromatism are perfectly corrected, realising the nearly identical excellent performance for the whole aperture.

For conventional applications, the longitudinal correction (A) and (B) are sufficient, because the observation is only operated with the full aperture. However, for recent fluorescence microscopy with laser excitation, if the light source has apodisation, such as Gaussian distribution, the effective NA would be narrowed. Moreover, the chromatic aberration and SA would increase tremendously if the spherochromatism and zonal error are not corrected. Concerning the special objectives with adjustable iris, this problem is more critical. Therefore, longitudinal aberration correction with the highest level (C) is preferred in the recently developed high-performance objectives.

The zonal error could be controlled only if the SA is corrected by the compensation between the primary contribution and the higher-order contribution [13]. According to Section 2.2, the correction of spherochromatism is associated with the higher-order SA and ACA contribution. Therefore, in the high NA microscope objectives, special techniques are applied to generate extraordinary higher-order contributions. In this section, both the basic cementing method correcting spherical and ACAs and the special features generating extraordinary higher-order aberrations, such as Merte surface and air lens, are introduced.

## 5.1 Cemented lenses

In the classical optical design theory, the functionality of a cemented lens in correcting SA and ACA is well described [13]. The optical power distribution and material are appropriately selected for the negative and positive components to generate arbitrary SA and ACA contribution. By cementing the two parts together, large amount of higher-order SA generated in the air gap could be removed, which improves the element sensitivity. However, in the high NA microscope objective, special Merte cementing is often applied to exploit the higher-order SA without hampering the element sensitivity.

The Merte surface [26, 27] is a heavily curved cementing surface, which is formed by two materials with small refractive index gap in the range of 0.05–0.15. In an example  $98 \times / 1.30$  oil immersion objective [28] shown in Figure 17, the second cemented doublet consists of the positive lens made of FK52 ( $n_d = 1.486$ ,  $v_d = 81.61$ ) and the negative element with N-LLF6 ( $n_d = 1.532$ ,  $v_d = 48.87$ ). Utilising the small index difference of 0.05 and large Abbe number ratio of 1.67, the doublet introduces extraordinary higher-order SAs and corrects ACAs simultaneously. Notably, the air gap between the front group and the middle group forms an air lens, which also introduces significant higher-order SA. A detailed introduction of this lens module would be given in 5.2.

When the Merte surface is removed by using a single FK52 lens in the middle group, changing the system from Figure 18A to B, the new system could still achieve the same SA correction of green light at full aperture. However, due to the lack of the higher-order contribution, the zonal error cannot be controlled. Furthermore, although the chromatic aberration is still well corrected at outer aperture for blue and red light, the system suffers from residual zonal error of all colours. Consequently, the resulting spherochromatism is also far worse than the original design.

As introduced in Section 3.2, for the ach-/apochromatic correction, the materials should be selected with a large Abbe number ratio and close partial dispersion. In fact, the typical selections already include many

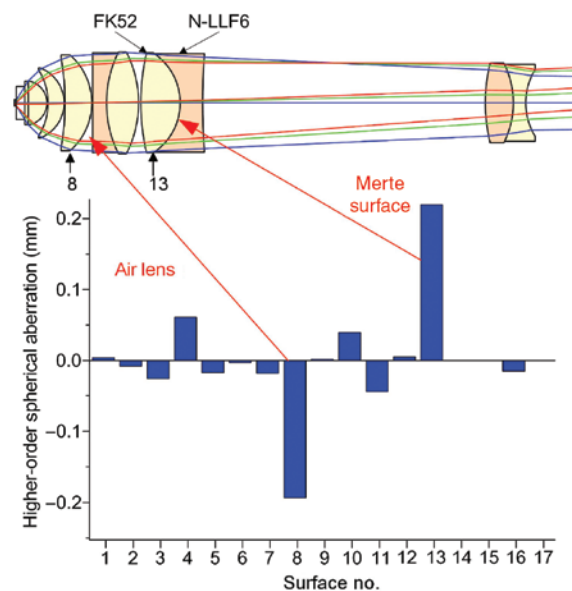


**Figure 17:**  $98 \times / 1.30$  oil immersion objective with the Merte cementing in the middle group, which introduces extraordinary higher-order SA.

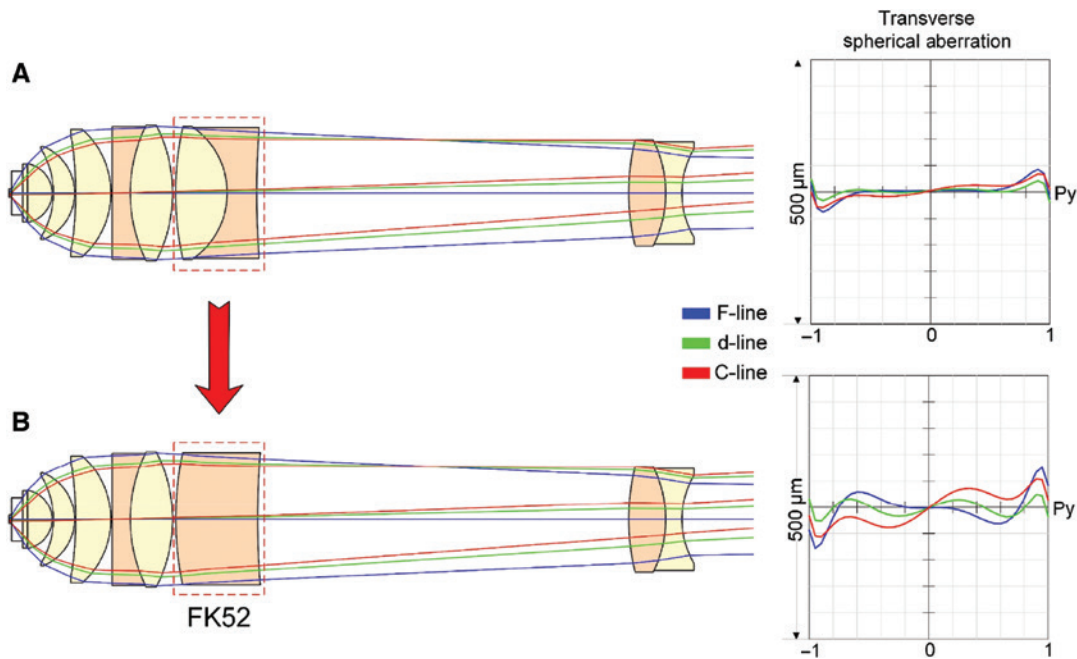


**Figure 18:** Comparison of systems with and without the Merte surface. (A) Original design with the strong curved cemented surface. (B) Changing the cemented doublet to a single lens, reoptimised system.

promising glass pairs to realise Merte cementing, which is summarised in Table 6. The combination of GFK/PK glass and short flint glass is the most popular solution.

### 5.1.1 Cemented doublets

The cemented doublet, which has been utilised since the traditional two-group objectives, is the most classical cemented lens and can be found in all the microscope objectives. For most cases, cemented doublets have positive optical power, which is cemented by a bi-concave or meniscus negative flint lens and a bi-convex positive crown glass. However, corresponding to some special consideration for aberration compensation and power distribution, the whole cemented doublets could be designed with meniscus shape providing slight negative

power. We classify the surface cementing into four types. The surface cementing types could also be applied to cemented triplets, which shall be introduced in 5.1.2.

1. Typical achromatic glass selection with weak surface cementing (weak surface bending)
2. Typical achromatic glass selection with strong surface cementing (strong surface bending)
3. Special glass selection with Merte surface cementing
4. Negative cemented doublet with weak optical power

The functionalities of these cemented doublets could be illustrated by the example 60×/1.45 oil immersion objective [29] shown in Figure 19, in which all the four types are used in the middle group. The objective apochromatically corrects the working spectrum from g-line to C-line, corresponding to the class (c) level.

**Table 6:** Popular glass pairs for the Merte cementing.

Glass Pair	Refractive index difference ( $\Delta n_d$ )	Abbe number difference/ratio ( $\Delta v_d$ )	Partial dispersion difference ( $\Delta P_{gf}$ )
GFK70, E-F2	0.051	35.05/1.95	0.042
GFK68, N-KZFS11	0.047	25.80/1.62	0.015
N-PK51, N-KZFS4	0.087	32.31/1.73	0.019
N-PK51, N-KZFS11	0.111	34.41/1.82	0.021
S-FPL51, N-KZFS11	0.143	38.83/1.92	0.023
Fluorite, S-NSL3	0.084	36.33/1.62	0.012
Fluorite, N-SK5	0.150	33.96/1.56	0.002
E-SK5, F9	0.031	23.08/1.61	0.054



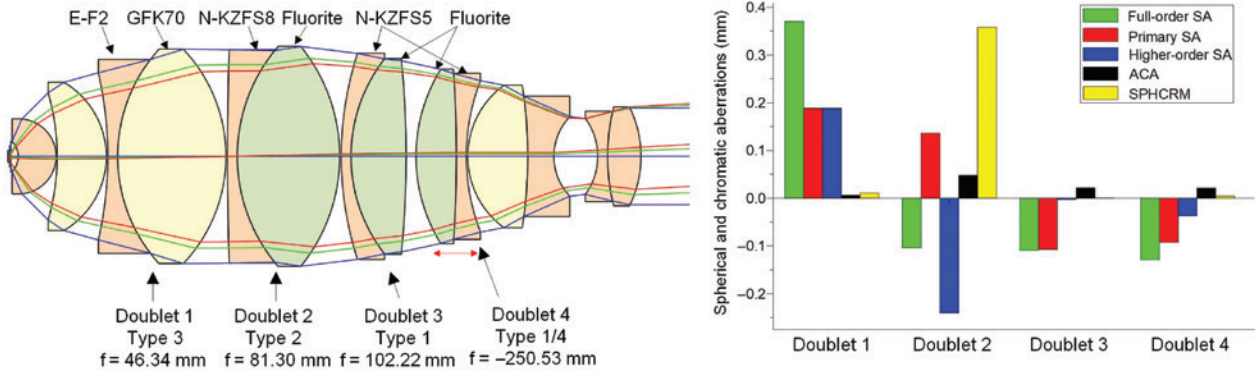


**Figure 19:** 60x/1.45 oil immersion objective utilising all the four types of cemented doublet with their aberration contributions, including primary and higher-order of SA, ACA (g-C) and spherochromatism (SPHCRM, g-C). The red arrow indicates the movable component for CORR functionality.

The first doublet is realised by cementing the negative component made of E-F2 ( $n_d=1.620$ ,  $v_d=36.26$ ) and the positive component made of GFK70 ( $n_d=1.569$ ,  $v_d=71.31$ ). Therefore, it forms a Merte cementing by the small index gap and strong surface curvature and generates nearly equivalent amount of primary and higher-order SA. The doublet 1 is located between the front group and the middle group. To smoothen the ray path, the fast doublet is designed with quasi-concentric front surface. Thus, it also has a similar functionality as the lens module No. 3 of the front group, which is an aplanatic shell-lens. However, to relax the design, the doublet is typically not used to compensate the chromatic aberration from the front group. The powers of the E-F2 and GFK70 lenses are carefully selected to fully correct the ACA within this element.

The material selection in the second and third doublet follows the basic achromatic and apochromatic principle, which has been introduced in Section 3.2. The fluorite ( $n_d=1.434$ ,  $v_d=95.26$ ) is utilised in both doublets as the positive component, but doublet 2 selects N-KZFS8 ( $n_d=1.720$ ,  $v_d=34.70$ ) for the negative component, while the doublet 3 utilises N-KZFS5 ( $n_d=1.654$ ,  $v_d=39.70$ ). The fluorite and the KZFS short flint glass have distinctive Abbe number, but similar partial dispersions within the selectable area (the g-line and F-line partial dispersions between 0.535 and 0.58). Therefore, the doublet 2 and doublet 3 could significantly introduce positive ACA contribution with suppressed secondary spectrum. Thus, the tremendous negative chromatic aberration introduced by the front group can be compensated. However, compared with type 1 doublet 3, due to the larger index gap between the two materials and the stronger curvature (associated with incidence angle), the type 2 doublet 2 leads to

critical marginal ray bending on the cemented surface, resulting in tremendous higher-order SA contribution, which is similar to the functionality of the Merte surface. According to Figure 19, doublet 2 introduces overcorrected higher-order SA that compensates the under-corrected primary contribution as well as the residual higher-order terms. On the contrary, although the height and incidence angle of marginal ray is nearly identical, the doublet 3 is almost free of higher-order SA due to the weak cemented surface. It is also notable that the doublet 2 has significant contribution to the spherochromatism correction, particularly on the rear surface, which forms an air lens with doublet 3. Its functionality will be introduced in 5.2.

The fourth doublet is composed with the same materials as doublet 3, but it has very weak negative optical power. Owing to the apochromatic material selection, the doublet 4 also has significant axial chromatic contribution. According to Figure 19, the element is sensitive to both the primary and higher-order SA. Thereby, the longitudinal movement of this component is utilised to realise the CORR function for cover glass thickness, corresponding to the power distribution type (e) shown in Table 2.

### 5.1.2 Cemented triplets

When it comes to the cemented triplet, there are two basic structures: the PNP cemented triplet, which is typically positive, and the NPN cemented triplet, which is typically negative, as shown in Figure 20.

The PNP triplet usually consists of a biconcave negative lens in the middle and two biconvex positive lenses at two sides. The NPN has two major subtypes: (1) the bi-convex positive lens in the middle and two meniscus negative lenses at two sides and the (2) bi-convex

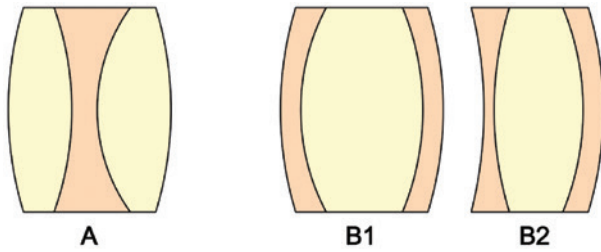


Figure 20: (A) PNP cemented triplet (B1), (B2) NPN cemented triplet.

positive lens in the middle with a meniscus negative lens at one side and a bi-concave negative lens at the other side, which are illustrated as (B1) and (B2) in Figure 20, respectively. The basic material selection method follows the same rule for chromatic correction introduced above. Due to the large refractive indices of the outer flint glasses and the low refractive index of the inner crown glass, the cemented triplet with a positive lens shape could realise negative power. According to the discussion in Section 6 of Part I, generally, the cemented doublet and triplet could achieve equivalent functionality in the SA and ACA correction. However, applying the triplets can save space for objectives with short parfocal length and relax the requirement of surface coating, while utilising the doublets could relax the element manufacture tolerance.

Different from the correction strategy of the system, which only utilises positive cemented doublets, when the triplet is used, optical designers usually create two cemented triplets with positive and negative power, respectively. These two cemented lenses compensate each other, and the residual difference is utilised to correct the

aberration from other groups. Thereby, the type (d) power distribution in Table 2 can be realised to relax the rear group. Figure 21 demonstrates an example  $63\times/1.20$  water immersion objective [30], where this correction strategy is applied. In the middle group, a PNP positive triplet and NPN negative triplet maintain SA with different signs, while both chromatic contributions are positive. Compared with the strategy to fully correct aberrations within one triplet, simply using the residual error for compensation could achieve better results, which corresponds to the strain' design consideration [31].

Notably, in some patented entries, the PNP triplet can also be designed with negative optical power. In the example  $40\times/1.20$  water immersion objective [32] shown in Figure 22, the second triplet selected FPL53 ( $n_d=1.439$ ,  $v_d=94.96$ ) for the two positive elements and S-LAL59 ( $n_d=1.734$ ,  $v_d=51.47$ ) for the negative middle lens. To correct the SA, including the ZSA, the two inner cemented surfaces have strong curvature, while the outer surfaces are weakly curved. Hence, the high index middle lens has great negative power ( $f=-6.87$  mm) and the two low index positive lenses have relatively weak power ( $f=15.55$  mm and  $f=22.82$  mm). Consequently, the overall focal power of this PNP triplet is negative. According to the surface aberration contributions, the overall SA of the two PNP triplets have different sign, which is the same as the typical case with a pair of PNP and NPN triplets. However, the two cemented surfaces both generate negative SA, which is different from the normal NPN negative triplet. Consequently, the four cemented surfaces of the two PNP objectives could generate larger higher-order SA, which is helpful in correcting the ZSA and spherochromatism.

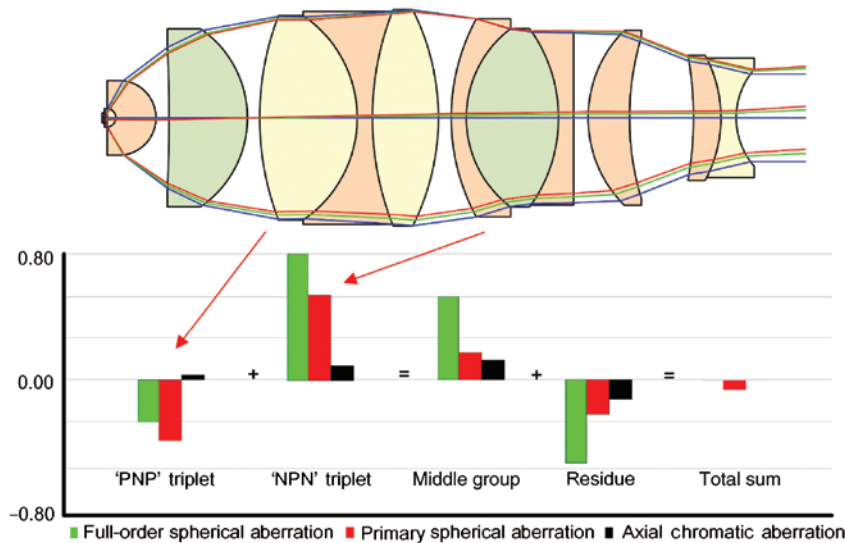
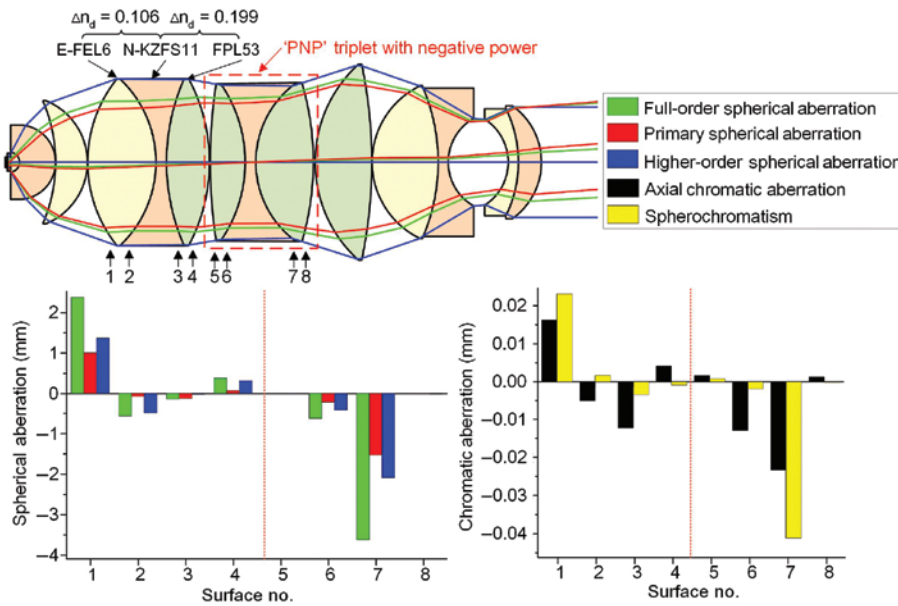


Figure 21: Typical  $40\times/1.20$  water immersion objective with a pair of PNP and NPN cemented triplets in the middle group.



**Figure 22:** 40 $\times$ /1.20 water immersion objective with two PNP cemented triplets in the middle group. The first normal PNP positive triplet uses both the normal cementing (type 1) and the Merte cementing (type 3), while the second PNP negative triplet only uses normal cementing (type 1 and type 2).

The Merte surface could also be utilised in the cemented triplet. Concerning the first cemented triplet in Figure 22, the front cementing belongs to type 3 Merte surface, which is formed by E-FEL6 ( $n_d = 1.532$ ,  $v_d = 48.84$ ) and N-KZFS11 ( $n_d = 1.638$ ,  $v_d = 42.41$ ) with a small index gap, while the third lens is made of FPL53, forming a type 1 cementing. Regarding the SA contributions of these two surfaces, the normal surface is primary-dominant, while the extraordinary Merte surface is higher-order dominant.

The cemented triplet could also be designed with weak power (type 4). Taking the advantage of the further enhanced chromatic correction, they are typically used in the middle group to realise CORR function, corresponding to the type (e) and type (g) power distribution in Table 2. Thereby, under different environmental conditions, despite the SA, both the focal length and chromatic correction could be kept, reaching the highest level of CORR. When the triplet is used in the centre of middle group, it is usually designed with the structure (A) and (B1) in Figure 20. When it is placed between the middle group and the rear group, structure (B2) is often applied.

### 5.1.3 Arrangement of the cemented lenses

Apart from the individual functionalities of the cemented lenses, the arrangement of these components in the middle group is also important, which is mostly based

on four considerations: (1) aberration compensation, (2) smoothing the ray path, (3) special optical power distribution and (4) manufacture and technology.

The consideration of aberration compensation could be seen from the examples in Sections 5.1.1 and 5.1.2. For one thing, systems like the example in Figure 19 suppressed the aberration contribution in each doublet. The element sensitivity can be reduced, but more components should be used. For another, according to the examples in Figures 21 and 22, applying the strain design idea by using two cemented triplets with opposite aberration behaviour, better correction can be realised with a smaller number of components, but the element sensitivity gets critical.

To restrain the unexpected aberration generated in the middle group due to large marginal ray height, the ray path should be smoothed. Therefore, the cemented elements between the middle group and the front group (or the rear group) could be designed with meniscus shape, which also provides similar functionalities as the adjacent group, e.g. the doublet 1 in the example shown in Figure 19. Furthermore, according to Section 2.2, arranging the middle group with quasi-symmetric ray path, it is also feasible to correct the coma, which can relax the design of the rear group.

Regarding the special power distribution types, particularly for the CORR objectives, weak power type 4 cementing should be utilised to achieve the

focal-length-invariant and chromatic-correction-invariant performance, when the objective is adjusted for environmental change.

The last consideration of manufacturing and technology has been discussed in Section 6 of Part I. In the examples shown in Figures 21 and 22, as a smaller number of elements are used, the design can match the 45 mm parfocal length, while the example in Figure 19 should use the 60 mm parfocal length. Furthermore, comparing one cemented triplet with two cemented doublets as equivalence, two strongly curved glass-air interfaces could be avoided. Thereby, the requirement of surface coating is relaxed.

In summary, the choice of optical designs in arranging cemented doublets and triplets mostly depends on the application requirement, aberration correction strategy and their manufacturing techniques.

## 5.2 Air lens

According to Section 5.1, the Merte surface generates extraordinary higher-order aberration with looser system tolerance due to its reduced element centring and positioning sensitivity. Despite the Merte surface, another powerful tool to generate higher-order terms is the air lens, which is a special air gap formed by two adjacent lens surfaces.

The functionality of the air lens, which generates higher-order contribution to correct ZSA and spherochromatism, is schematically demonstrated as Figure 23. To effectively correct the ZSA there must be a large amount of SA in the air gap, so that the marginal ray drops rapidly as compared to the zonal rays. The air gap, therefore, under-corrects the marginal aberration more rapidly than the zonal aberration. Thus, when the index step of the two materials gets larger and the two glass surfaces are strongly curved, this effect becomes more potent.

When it comes to the spherochromatism correction, considering an air gap formed by a broken cemented

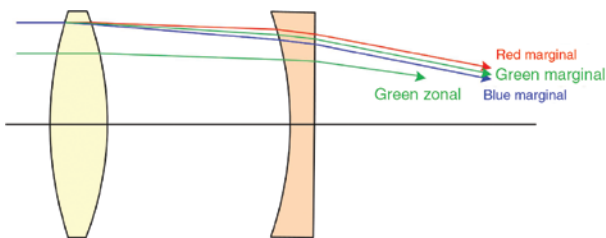


Figure 23: Mechanism of spherochromatism correction with air lens.

achromatic doublet, when the achromate is still cemented, the outer surfaces contribute to the under-correction of SA and the cemented surface has a strong over-correction for compensation. The contribution is related to the index step at the cemented surface. This balancing to a zero sum is valid for the central wavelength (green). On the blue side, the refractive indices are higher, and the dispersion is larger than that on the red side. The over-correcting effect of the cemented surface is too large in the blue and too small in the red. If the two lenses are separated by an air gap, the blue ray has a smaller height at the second lens and its spherical contribution decreases. In comparison to the central wavelength, the opposite effect happens in the red. This compensates the spherochromatism and thus offers the possibility to correct it [27].

We can conclude two conditions of an air gap to correct spherochromatism and ZE, presenting the effect of an air lens:

1. Strongly curved surface and/or large index step
2. Ach-/apochromatic choice of glasses

When the first condition is fulfilled, the air lens contributes greatly to the ZSA control. With the additional second condition, it is more beneficial to correct spherochromatism. In the microscope objectives, these two conditions are easily fulfilled, corresponding to the utilisation of the cemented lenses with appropriate glass choice and strongly curved outer surface. There are two types of air lens utilised in the middle group: the natural air lens and the artificial air lens.

The natural air lens is formed by the small air space between the cemented lenses. Figure 24 demonstrates the same example as discussed in Figure 17. Apart from the Merte surface in the second doublet, the gap between the FK52 ( $n_d = 1.486$ ,  $v_d = 81.61$ ) lens and the LAF11 ( $n_d = 1.757$ ,  $v_d = 31.70$ ) lens forms an air lens generating enormous higher-order SA, which is beneficial in achieving ZSA correction. Furthermore, these two materials with a large difference of dispersion fulfil the achromatic condition. Consequently, the air lens also works well for the spherochromatism correction. On the contrary, another colour-free natural air lens is formed by the two doublets with FK52 glass. As there is no index gap and dispersion difference, the air lens is free of chromatic aberration and only has small higher-order contribution.

A new technique, which appeared in the recent decade, is generating artificial air lens with special reverse bent structure in the middle group. Figure 25 gives an example  $25\times/0.80$  water immersion objective [33]

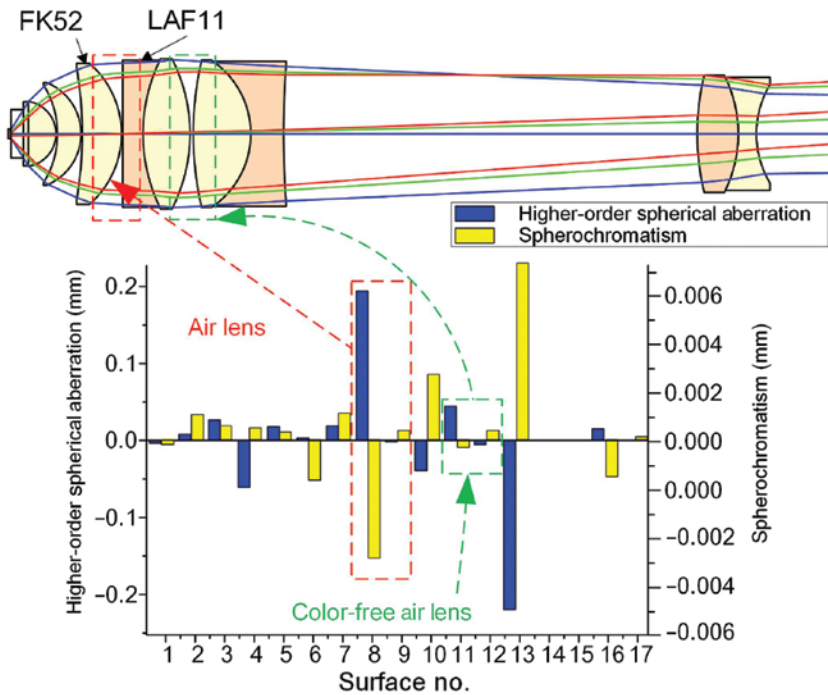


Figure 24: 98x/1.30 oil immersion objective with two natural air lenses.

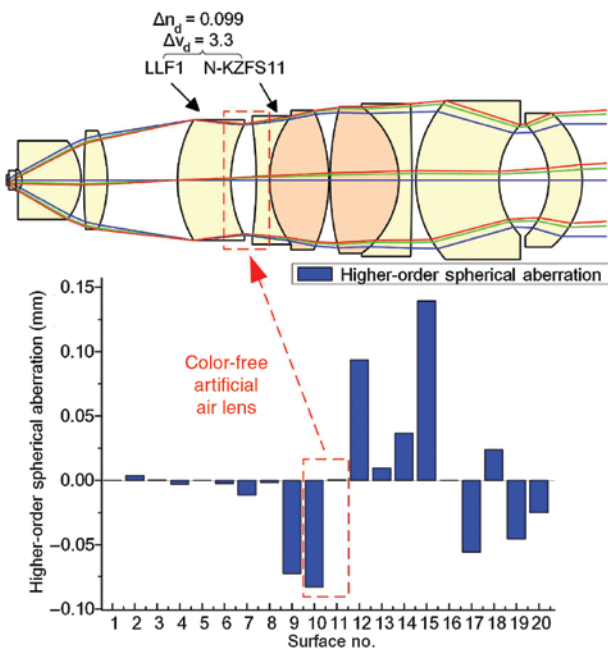


Figure 25: 25x/0.80 water immersion objective with artificial air lens.

with a reverse bent lens, which only has the functionality of spherical control. These two selected glasses LLF1 ( $n_d = 1.548, v_d = 45.75$ ) and N-KZFS11 ( $n_d = 1.638, v_d = 42.41$ ) have similar dispersions. Therefore, the air lens is free of chromatic aberration and only corrects ZSA.

Notably, the front surface of the reverse bent lens also holds significant higher-order SA contribution and the focal power of the lens is very small. Therefore, this element is used to realise the cover glass thickness CORR function for this objective with type (f) power distribution.

In conclusion, in conventional applications with air lens, the optical designer should be careful in adjusting the air gap to avoid the introduction of higher-order terms. The presence of the higher-order aberration makes the lens less tolerant to manufacturing and alignment errors. On the contrary, the modern microscope objective often utilises air gaps with higher-orders to adjust the system SA. As the thickness of the air lens significantly influences its effect for correction, it is possible to use it as a compensator to balance the manufacturing error or environmental change.






### 5.3 Summary

The nine lens modules utilised in the middle group are summarised in Table 7 in terms of their functionalities in correcting the four major aberrations: SA, ZSA, ACA and spherochromatism (SPHCRM). Furthermore, the special impacts of application and considerations of manufacturing and technology are also marked.

**Table 7:** Summary of lens modules in the middle group.

No.	Lens modules	Aberration correction				Application/ Manufacturing and technology considerations
		SA	ZSA	ACA	SPHCRM	
1	Weak ach-/apochromatic cement		–			–
2	Strong ach-/apochromatic cement					Difficult to cement
3	Merte surface					Difficult to cement
4	Cemented lens with weak power					CORR
5	Meniscus cemented lens between front and middle group		–			Relax system with smooth ray path
6	Meniscus cemented lens between middle and rear group					Relax system with smooth ray path, CORR
7	Cemented triplet					Relax coating, save space
8	Air lens (natural/artificial)					CORR
9	Colour-free air lens			–	–	CORR

	Great positive effect		Significant positive effect		Slight positive effect
	Slight negative effect		Significant negative effect	–	Negligible effect

## 6 Lens modules in the rear group

According to the historical review [1], the creation of the rear group originated from the weak power thick meniscus lens invented by Boegehold in 1938, which purely compensates the FC. In the 20th century, Plan-objectives were further developed with advanced rear group structure, which corrects the FC and controls the lateral chromatic aberration with weak or negative optical power. Conventionally, the slight coma and astigmatism can also be compensated by the rear group. However, during the recent development, due to the extension of system etendue, highly sophisticated rear groups are utilised to suppress coma and correct SA. Therefore, the rear group becomes the most complicated part in the modern microscope objectives. Its structure significantly determines the achievable system parameter. Notably, a few special designs combined the functionality of the middle group and the rear group to form a sensitive but effective rear group for aberration correction, e.g. 100×/1.20 oil immersion objective designed by Sharma [34]. These systems (4 entries) are considered as exceptions to our analysis and they are thus excluded from this paper.

### 6.1 Principle of field flattening and lateral colour control

The front and middle groups of the microscope objectives are designed mostly with positive components to provide

strong positive power and correct ACA. Although the embedded front lens could have a positive contribution, the residual Petzval curvature from the front and middle groups are always negative. Therefore, before the invention of Boegehold, there was always a contradiction between the field flattening and axial chromatic correction.

In the classical theorem of aberration correction [27], with purely refractive elements, there are three well-known methods to compensate the Petzval curvature:

1. Utilising the field lens close to the image or intermediate image;
2. Utilising the thick meniscus lens with positive Petzval curvature under arbitrary power; and
3. Petzval's theorem, utilising positive and negative elements widely apart from each other [35]

Typically, the first method is only used in the Zone 5 microscope objective with very low magnification, where the third method is also applied to correct the very large object field. The details will be introduced in Part III.

It is also well known that the exact FC should be understood with a combination of Petzval curvature and astigmatism. According to Petzval's theorem, when the third method is applied, the astigmatism can be corrected by the remote rear lenses. However, when it comes to the second method, the thick meniscus lens cannot correct astigmatism by itself. The Gauss type rear group is typically used, which is a quasi-symmetric setup consisting of two thick meniscus lenses. These two meniscus lenses are designed with strongly curved outer surfaces, on which the off-axis ray bundle could generate significant tangential

and sagittal difference as astigmatism contribution. Finely adjusting the asymmetry, the residual astigmatism from the front and middle groups can be compensated. Furthermore, the coma can be well controlled by the quasi-symmetric structure simultaneously if the stop position is appropriately selected.

When it comes to the control of lateral colour, based on the strategy of different manufacturer, it should be fully corrected or controlled around a fixed value, e.g. 1.5%. The condition of the lateral colour correction is given by Equation (9)

$$\sum_j \frac{\omega_{pj}}{\omega_j} \cdot \omega_j^2 \cdot \frac{F_j}{v_j} = 0, \quad (9)$$

where  $\omega_j$  represents the relative marginal ray height,  $\omega_{pj}$  is the relative chief ray height,  $F_j$  is the focal power and  $v_j$  is the Abbe number.

We can decompose the first term  $\omega_{pj}/\omega_j$  as the ray bundle separation contribution, and the second term  $\omega_j^2 \cdot F_j / v_j$  as the axial colour contribution. To generate a large contribution in the rear group for compensation, the ray bundle separation of fields should be as large as possible and the glasses should be carefully selected to introduce appropriate axial colour. The typical achromatic materials are sometimes selected to better adjust it. In this section the lateral colour is analysed for the spectrum of F-line to C-line.

## 6.2 Basic structures and lens modules

According to 3.1, the functionality of the rear group in correcting SA mostly depends on the power distribution, which is related to the optical power of the rear group and relative marginal ray height. As it is nearly independent of the structure, in this section, we only focus on the basic lens modules for coma, astigmatism, FC and chromatic aberration correction. Some special lens modules for SA correction will be discussed in Section 6.3. Based on the principle of field flattening and lateral colour correction, the rear groups are designed with three basic structures: single element (possible cemented), quasi-symmetric Gauss type and separated positive and negative components (Petzval type), which are shown in Figure 26.

The type (A) rear group with single meniscus element is the most classical rear group. It could be designed with negative or very weak power, which is composed of a single meniscus lens or two components cemented together. As the chief ray height is relatively large on this element, it can significantly contribute to the coma

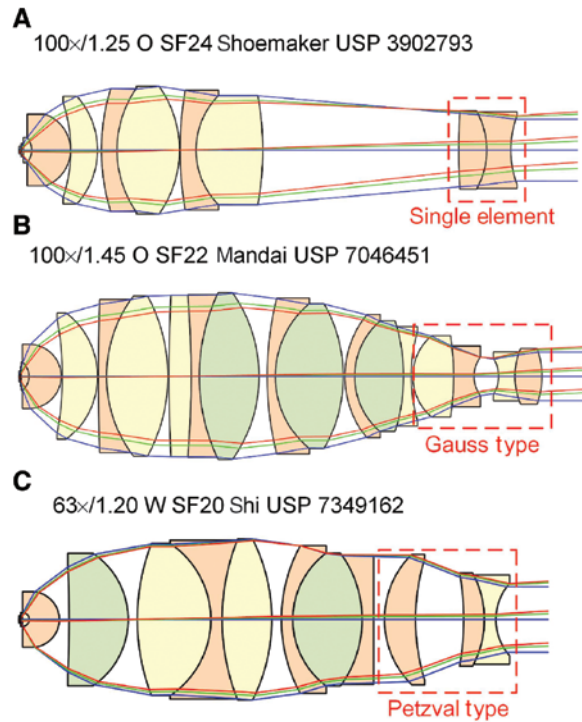


**Figure 26:** Three basic rear group structures. (A) Single meniscus lens, including cemented meniscus lens. (B) Gauss type quasi-symmetric setup with two thick meniscus lenses. (C) Petzval type with separated positive and negative components.

correction. However, to avoid generating higher-order coma, the single element should be placed with its concave surface facing the image side [9]. However, the single element cannot be designed with strongly curved outer surfaces to restrain SA; thus, it is difficult to compensate astigmatism with this structure. Therefore, the type (A) rear group is not applied to the Zones 3 and 4 systems with relatively high etendue, in which the astigmatism is more critical. Due to the excellent sensitivity and low cost, it is widely used in the Zone 2 systems with low or medium etendue. It is particularly useful in the high-magnification long working distance objectives with the retrofocus structure.

The type (B) quasi-symmetric Gauss type rear group is the most popular setup in the modern high NA microscope objectives, particularly for the applications with immersion. Two single or cemented meniscus lenses with strongly curved outer surfaces are used, which is similar to the middle part of classical double-Gauss photographic objectives. Although the stop aperture cannot locate between the two groups realising perfect symmetry, this setup can still fine adjust coma and lateral colour according to symmetry principle and control the astigmatism with the strong curvatures. However, due to the great ray

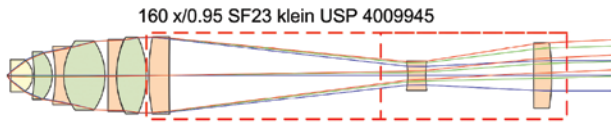


**Figure 27:** First three-group microscope objectives with Petzval type rear group.

bending in the air gap, the element is very sensitive to centering error. Moreover, the strongly curved surfaces also require tight surface figure tolerance. Consequently, the cost of the Gauss type rear group is relatively high.

The type (C) Petzval type rear group can balance the cost and correction level, which was firstly reported by Klein in 1967 [36], as shown in Figure 27. The very early development utilised the conventional Petzval structure with two positive lenses and a negative lens forming a PNP structure, which well corrects both the astigmatism and Petzval curvature. However, since the three components should be placed far from each other, the objective cannot be parfocalised. In the recent developments, such as the example shown in Figure 26C, the advanced Petzval type rear group with separated positive and negative components are used, by which the FC and coma are well corrected. Compared with the Gauss type, it is less sensitive. For some special cases, the Petzval type rear group can also be designed sensitive by applying air lens effect, which is useful to realise CORR function. It will be further introduced in Section 6.3. The drawback of this structure is that the higher-order coma is hard to control, thus it is not used in the Zone 4 systems with extremely high etendue.

Utilising these three basic structures, historically, the distance between the middle group and rear group was enlarged to control the lateral colour. The longer separation exploits the first term of Equation (9). The light propagates along the long air distance and creates a

larger separation of chief ray away from the optical axis, thus the rear group significantly contributes to lateral colour correction. As illustrated in Figure 28, there is a 25.52 mm-long separation between the middle group and rear group of the 40 $\times$ /0.65 objective [37]. Moving the rear group towards the middle group by 6 mm and reoptimising the rear group to realise the same resolution, the lateral colour from the tube lens, front and middle group nearly remain the same, but the contribution from the rear group significantly drops, resulting in the under corrected lateral chromatic aberration.

However, in the highly sophisticated objectives with extended etendue, more components are used in the middle group, which requires large axial space. To match the standardised parfocal length, the air spacing between the middle and rear group is limited. Therefore, thick lenses made of high index materials are often used to achieve large ray bundle separation with reduced distance. In the example 63 $\times$ /1.00 water dipping objective with type (b) rear group [38] as shown in Figure 29, the thick S-LAH59 ( $n_d=1.816$ ,  $v_d=46.62$ ) meniscus lens effectively separates the off-axial ray bundles and the last S-NBH51 ( $n_d=1.750$ ,  $v_d=35.30$ ) meniscus lens contributes significantly to the lateral colour control. Notably, according to Kingslake and Johnson [13], it is possible to thicken a lens element by providing a large amount of under-corrected SA within the glass, which could be used to reduce ZSA. Thus, when the marginal ray height in the rear group is high, the thick lens could also effectively contribute to SA correction, ZSA correction and even achromatisation [39].

According to Equation (9), controlling the lateral colour is also associated with the ACA of the rear group. In the conventional Zone 1 and Zone 2 systems, due to the small NA and field size, the residual lateral colour from the front group and middle group is not critical. Therefore, achromatic glasses are usually selected. Concerning the example

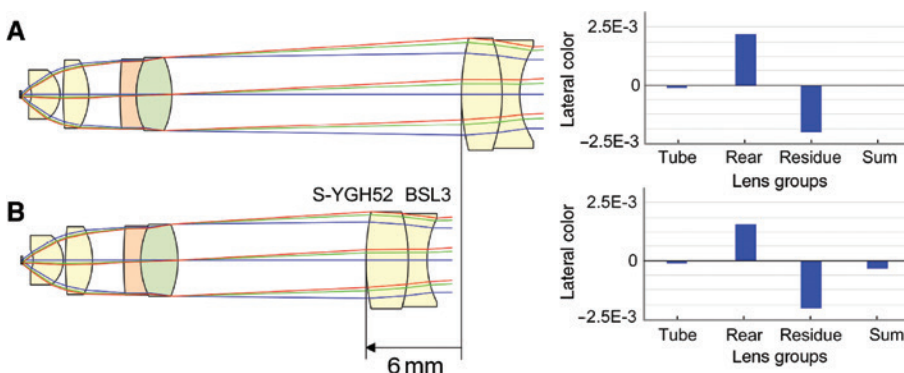


**Figure 28:** Lateral colour correction with long separation of middle and rear group of a 40 $\times$ /0.65 objective. The cemented single meniscus rear group consists of two crown glasses as S-YGH52 and BSL3. (A) Original design with excellent compensated lateral colour. (B) Reoptimised system with reduced separation and hampered lateral colour correction.



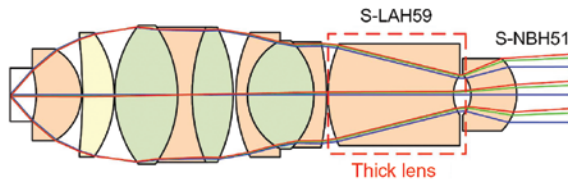


**Figure 29:** Ray bundle separation with thick lens with high refractive index in  $63\times/1.00$  water dipping objective.

system in Figure 28, the rear doublet is cemented by a Middle Glass S-YGH52 ( $n_d = 1.787$ ,  $v_d = 50.00$ ) with flint behavior and a typical crown glass BSL3 ( $n_d = 1.498$ ,  $v_d = 65.03$ ). To realise the achromatism of the negative doublet, the positive element is made of flint S-YGH52, while the negative component is designed with low dispersive crown BSL3.

When it comes to the system suffering from large residual lateral colour, to further increase the contribution of rear group, it is necessary to enlarge the second term of Equation (9) of axial colour contribution. Therefore, the SF glasses with high index and large dispersion are widely used, which is the so-called SF principle. According to Section 3.2, due to the consideration of general colour correction and autofluorescence suppression, the medium dispersion SF glasses are most favourable, e.g. the S-LAH59 and S-NBH51 used in the Figure 29 example system. The SF lenses also generate residual ACA, which should be compensated by the middle group. It is notable that the SF glasses usually have relatively low transmittance in UV range. Therefore, when they are used in the objectives for UV applications, such as UV fluorescence excitation, the lens thickness should be reduced.

To finely adjust the chromatic aberration, as a special approach, the cemented doublets used in the rear group can be designed with buried surface. The buried surface is formed by two cemented elements with nearly identical refractive indexes but distinctive dispersions. By simply

controlling the curvature of the cementing surface, the chromatic aberration is adjusted without disturbing monochromatic aberrations. Therefore, cementing two SF glasses is an efficient technology to control lateral colour. An example  $60\times/1.40$  oil immersion objective is shown in Figure 30.

Based on the quasi-symmetric structure with strongly curved surfaces, the coma, astigmatism and Petzval curvature of the rear group are well balanced. However, because of the distinctive glass selection, the chromatic aberration does not show symmetric behaviours over the six surfaces. The first cemented meniscus doublet selects typical achromatic material GFK70 ( $n_d = 1.569$ ,  $v_d = 71.32$ ) and S-LAH63 ( $n_d = 1.804$ ,  $v_d = 39.59$ ), while the second meniscus doublet is comprised of S-LAH63 and FD60 ( $n_d = 1.805$ ,  $v_d = 25.46$ ), thus forming a buried surface. Consequently, the second cementing surface only contributes to chromatic correction. This cemented lens takes advantage of both the SF principle and buried surface.

### 6.3 Advanced lens modules

When the system etendue is extended, the exit pupil size is enlarged and the marginal and coma ray heights in the rear group increase, resulting in inevitable SA. To compensate the tremendous SA between the middle and rear groups, particularly concerning the higher-order contribution for ZSA correction, advanced lens modules should be utilised.

The same as the middle group, the air lens is the most effective tool to generate extraordinary higher-order SA. However, different from the middle group, the rear group lacks the natural air lens, which is usually formed by the cemented lenses with strong outer curvature in the middle group. Typically, only an artificial air lens is seen in the rear group. Figure 31 demonstrates a  $40\times/1.00$  water immersion objective [40] utilised a natural air lens in the middle group and an artificial air lens in the rear group. The rear group

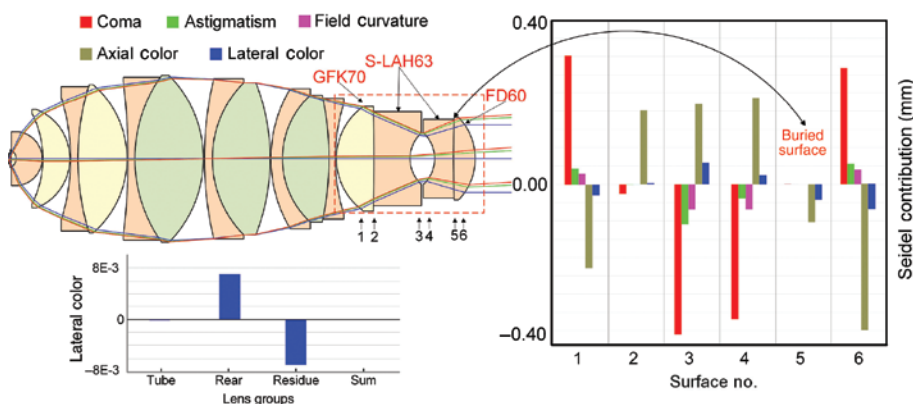


**Figure 30:**  $60\times/1.40$  oil immersion objective with buried surface cementing in the rear group.

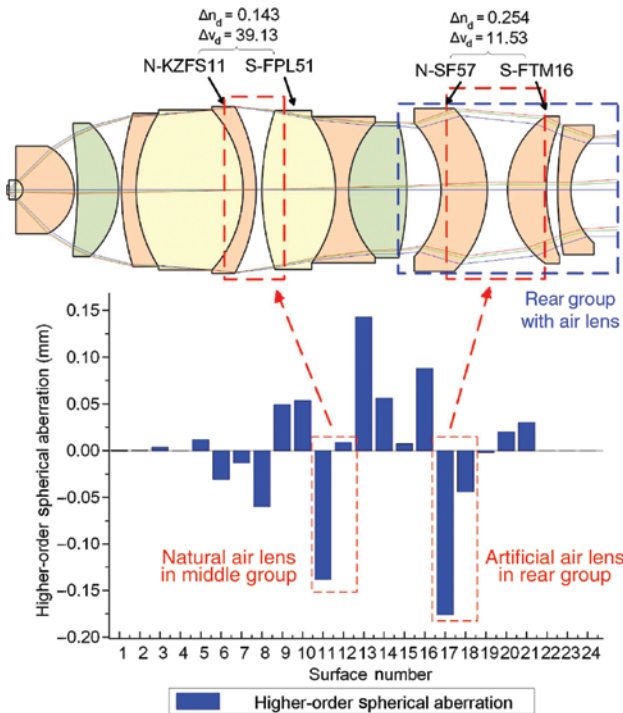


**Figure 31:** 40x/1.00 water immersion objective with natural air lens in the middle group and artificial air lens in the rear group for SA and ZSA correction.

belongs to the basic structure type (c), which consists of separated elements made of flint glasses, with weak, positive and negative optical power. The S-FTM16 ( $n_d = 1.593$ ,  $v_d = 35.31$ ) meniscus lens and N-SF57 ( $n_d = 1.847$ ,  $v_d = 23.78$ ) meniscus lens forms a strong positive artificial air lens with large index gap, thus generating tremendous higher-order SA. The two cemented triplets in the middle group forms a natural air lens with smaller index gap, thus generating smaller higher-order contribution under similar marginal ray height and incidence angle. The artificial air lens in the rear group can also be used to realise the CORR function of the objective. Notably, as a byproduct, the Petzval type rear group with air lens may also generates higher-order coma. Therefore, this type of air lens is seldom used in the objectives with extremely high etendue.

When the system etendue is extremely high, the power distribution must be changed to type (c), consisting of quasi-symmetric part and an additional positive component. To avoid generating tremendous SA and higher-order coma, a positive meniscus lens with quasi-concentric front surface is usually added behind the Gauss group. Three high etendue objectives are shown in Figure 32 under the same scale.

The system (A) has the smallest etendue, where only a single meniscus lens is added to smoothen the ray path.

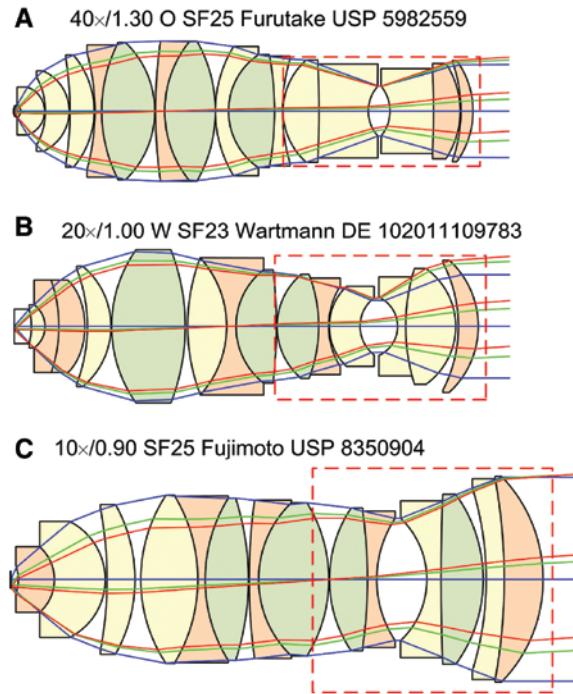


**Figure 32:** High etendue objectives utilising Gauss type rear group with additional lenses. (A) High etendue system with additional single meniscus lens behind the Gauss type rear group. (B) High etendue system with both additional meniscus lenses in front of the Gauss type rear group and behind the Gauss type rear group. (C) Extremely high etendue system with additional cemented meniscus lens behind the Gauss type rear group.

With nearly doubled etendue, the system (B) exploits greater bending of the additional lens and utilises more complicated quasi-symmetric structure. Concerning the system (C) with highest etendue, the additional lens is also designed as a cemented doublet, which is the common structure used in the state-of-the-art high etendue systems. The aberration correction functionalities of these complicated rear groups are very complicated. All the aberrations are involved, which cannot be clearly decoupled. Designing the Zone 4 extremely high etendue objectives always requires special consideration.

## 6.4 Summary

The ten lens modules utilised in the rear group are summarised in Table 8 in terms of their functionalities in correcting the aberrations: SA, ZSA, coma, astigmatism, FC, ACA and LCA. Furthermore, special impacts of application and consideration of manufacturing and technology are also marked.

**Table 8:** Summary of lens modules in the rear group.

No.	Lens modules	Aberration correction						Application/ Manufacturing and technology considerations	
		SA	ZSA	Coma	AST	FC	ACA		LCA
1	Single meniscus element (possibly cemented)	–	–	■	■	■	–	–	Low/medium etendue, low cost, insensitive
2	Quasi-symmetric Gauss type	–	–	■	■	■	–	–	Critical sensitivity
3	Petzval type	–	–	■	■	■	–	–	Possible CORR, medium sensitivity
4	Long separation between the middle and rear group	–	–	–	–	–	–	■	Hampering parfocalisation
5	Thick lens	■	■	■	■	■	■	■	–
6	Dense flint principle	■	–	–	–	■	■	■	–
7	Achromatic cementing	■	–	–	–	–	■	■	–
8	Buried surface	–	–	–	–	–	■	■	–
9	Air lens	■	■	■	■	–	■	■	CORR
10	Additional lens with Gauss type	■	■	■	■	■	■	■	High etendue

■	Great positive effect	■	Significant positive effect	■	Slight positive effect
■	Slight negative effect	■	Significant negative effect	–	Negligible effect

## 7 Conclusion

Defining an iterative paraxial raytracing method and selecting appropriate tools for primary and higher-order aberration contribution evaluation, the major Zones 1–4 microscope objectives are systematically analysed. The optical power distribution and material selection strategy are summarised and associated with the general aberration correction strategy. In each structural group, which is also a functional group for specific aberration restraint or correction, the lens modules are extracted and analysed. Here, 10 modules for the front group, 9 modules for the middle group and 10 modules for the rear group are well sorted. Apart from the aberration-related behaviour, some related application impacts and manufacturing and technology considerations are briefly discussed. Notably, producing the highly sophisticated microscope objective greatly depends on the manufacturers' technique, including the mechanical design. Therefore, aside from the summarised theoretical lens modules, the mechanical-related features and more detailed manufacturing and technology considerations should be analysed in future works.

Specific lens modules used in the very-low-magnification Zone 5 objectives and the very-high-magnification Zone 6 objectives have not been discussed. Furthermore, the discussion of special techniques for the CORR objectives and the utilisation of diffractive optical elements (DOE) are not included in this paper. These miscellaneous topics will be introduced in Part III, together with system synthesis examples, in which the summarised lens modules are utilised.

## References

- [1] Y. Zhang and H. Gross, *Adv. Opt. Technol.* 8, 303–337 (2019).
- [2] Y. Zhang and H. Gross, *Proc. SPIE* 10590, 105901G (2017).
- [3] H. H. Hopkins, in 'Applied Optics and Optical Engineering', (Academic Press, New York, 1983) pp. 307–369.
- [4] E. Delano, *J. Opt. Soc. Am.* 42, 631 (1952).
- [5] L. J. Danner, *USP* 4384765 (1983).
- [6] A. Berner, E. Kasperkiewicz, Y. Zhang and H. Gross, *J. Opt. Soc. Am. A Opt. Image Sci. Vis.* 35, 1368–1378 (2018).
- [7] C. Metz, *Zeitschr. für wiss. Mikroskopie.* 37, 49–52 (1920).
- [8] H. Boegehold, *US* 2206155 (1940).
- [9] T. Toshi and M. Akiko, *US* 8958154 (2008).
- [10] J. R. Rogers, *Adv. Opt. Technol.* 2, 41–51 (2013).
- [11] K. Suzuki, *JP* 2003-015046 (2003).
- [12] T. Tojyo, *US* 4280757 (1981).
- [13] R. Kingslake and R. B. Johnson, in 'Lens Design Fundamentals', (Academic Press, Burlington, 2009) pp. 179–184.
- [14] H. Konishi, *US* 5739957 (1998).
- [15] Y. Fujimoto and D. Nishiwaki, *US* 6747804 (2001).
- [16] H. Konishi, Y. Fujimoto, K. Kusaka and T. Kasahara, *US* 7486445 (2008).
- [17] Y. Saito, *JP* H05-142477 (1993).
- [18] M. Yamahiro, *JP* H11-174339 (1999).
- [19] H. Yamada, Y. Suenaga and I. Ito, *US* 5708531 (1998).
- [20] D. N. Frolov, O. A. Vinogradova, V. N. Frolov and P. S. Vakulov, in 'The Construction of Frontal Components of Objectives for Microscope: Optical Design', *Proceedings Volume 10690, Optical Design and Engineering VII*; 1069021, (SPIE Optical Systems Design, Frankfurt, Germany, 2018), <https://doi.org/10.1117/12.2311799>.
- [21] A. Mijs and J. Novak, *Appl. Opt.* 49, 3403–3410 (2010).
- [22] X. Lu, O. Rodenko, Y. Zhang and H. Gross, *Appl. Opt.* 58, 3589–3596 (2019).
- [23] Y. Fujimoto, *JP* 2006-113287 (2006).
- [24] K. Yamaguchi, *US* 7262922 (2005).

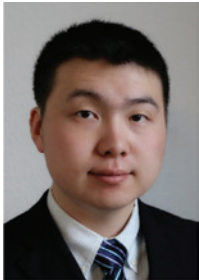
- [25] T. Bauer and C. Schulz, US 20140247502A1 (2016).
- [26] W. Merte, H. Richter and M. von Rohr, in 'Das Photographische Objektiv', (Springer, Wien, 1932) pp. 243–366.
- [27] H. Gross, H. Zügge, M. Peschka and F. Blechinger, in 'Handbook of Optical Systems, Vol. 3: Aberration Theory and Correction of Optical Systems', (Wiley, Weinheim, 2007).
- [28] W. Klein, US 3524694 (1965).
- [29] M. Mandai and K. Yamaguchi, US 7046451 (2006).
- [30] R. Shi, US 7349162 (2008).
- [31] D. Shafer, in 'Optical Design and The Relaxation Response', Proceedings Volume 0766, Recent Trends in Optical Systems Design and Computer Lens Design Workshop, (OE LASE'87 and EO Imaging Symposium, Los Angeles, CA, United States, 1987), <https://doi.org/10.1117/12.940196>.
- [32] M. Matthae, W. Kleinschmidt and G. Herbst, US 7268953 (2007).
- [33] R. Shi, I. Fahlbusch and W. Kleinschmidt, US 7782539 (2010).
- [34] K. D. Sharma, Appl. Opt. 24, 2577 (1985).
- [35] G. Franke, 'Photographische Optik', (Akademische Verlagsgesellschaft, Frankfurt am Main, 1964).
- [36] W. Klein, US 4009945 (1967).
- [37] K. Kajitani, US 6441966 (2002).
- [38] R. Wartmann and J. Sprenger, 20060018030 (2006).
- [39] H. Takenaka, 'Recent Trends in The Design of Microscope Objectives', Proceedings Volume 0554, 1985 International Lens Design Conference, Ed. By D. T. Moore, W. H. Taylor, (1985 International Lens Design Conference, 1985, Cherry Hill, United States, 1986), doi: 10.1117/12.949268.
- [40] R. Shi, et al., US 20130271847 (2013).



### Herbert Gross

Institute of Applied Physics, Friedrich Schiller University Jena, Albert-Einstein-Str. 15, 07745 Jena, Germany

Herbert Gross studied Physics at the University of Stuttgart. He received his PhD on Laser Simulation in 1995. He joined Carl Zeiss in 1982, where he worked as a scientist in optical design, modelling and simulation. From 1995 to 2010, he headed the Central Department of Optical Design and Simulation. Since 2012, he has been a professor at the University of Jena in the Institute of Applied Physics and holds a chair in Optical System Design. His main working areas are physical optical simulations, beam propagation, partial coherence, classical optical design, aberration theory, system development and metrology. He was editor and main author of the book series 'Handbook of Optical Systems'.



### Yueqian Zhang

Institute of Applied Physics, Friedrich Schiller University Jena, Albert-Einstein-Str. 15, 07745 Jena, Germany  
[yueqian.zhang@uni-jena.de](mailto:yueqian.zhang@uni-jena.de)

Yueqian Zhang completed his undergraduate study in Optical Engineering at Zhejiang University, Hangzhou, China. He received his Master's degree in Photonics from the Friedrich-Schiller-Universität Jena, Germany, in 2015. Since 2016, he has been working in the Optical Design Group at the Institute of Applied Physics in Friedrich-Schiller-Universität Jena. His research interests are classical system design, microscopic application and system development.